Final Draft
of the original manuscript:

Prylutska, S.; Panchuk, R.; Golunski, G.; Skivka, L.; Prylutskyy, Y.; Hurmach, V.; Skorohyd, N.; Borowik, A.; Woziwodzka, A.; Piosik, J.; Kyzyma, O.; Haramus, V.M.; Bulavin, L.; Evstigneev, M.; Buchelnikov, A.; Stoika, R.; Berger, W.; Ritter, U.; Scharff, P.:

C60 fullerene enhances cisplatin anticancer activity and overcomes tumor cell drug resistance

In: Nano Research (2016) Springer

DOI: 10.1007/s12274-016-1324-2

C_{60} fullerene enhances cisplatin anticancer activity and overcomes tumor cells drug resistance

Svitlana Prylutska[1A], Rostyslav Panchuk[2A], Grzegorz Gołuński[3A], Larysa Skivka[1], Yuriy Prylutskyy[1*], Vasyl Hurmach[1], Nadya Skorohyd[2], Agnieszka Borowik[3], Anna Woziwodzka[3], Jacek Piosik[3*], Olena Kyzyma[1,4], Vasil Garamus[5], Leonid Bulavin[1], Maxim Evstigneev[6*], Anatoly Buchelnikov[6], Rostyslav Stoika[2], Walter Berger[7], Uwe Ritter[8], Peter Scharff[8]

[1]*Taras Shevchenko National University of Kyiv, 64 Volodymyrska Str., 01601 Kyiv, Ukraine*

[2]*Institute of Cell Biology, NAS of Ukraine, 14-16 Drahomanov Str., 79005 Lviv, Ukraine*

[3]*Laboratory of Biophysics, Intercollegiate Faculty of Biotechnology UG-MUG, Abrahama 58, 80-307 Gdańsk, Poland*

[4]*Joint Institute for Nuclear Research, 6 Joliot-Curie Str., 141980 Dubna, Moscow reg., Russia*

[5]*Helmholtz-Zentrum Geesthacht: Centre for Materials and Coastal Research, 1 Max-Planck Str., 21502 Geesthacht, Germany*

[6]*Belgorod State University, 85 Pobedy Str., 308015 Belgorod, Russia*

[7]*Institute of Cancer Research and Comprehensive Cancer Center, Medical University Vienna, 1090, 8A Borschkegasse, Vienna, Austria*

[8]*Technical University of Ilmenau, Institute of Chemistry and Biotechnology, 25 Weimarer Str., 98693 Ilmenau, Germany*

[A] – These authors contributed equally to this work.

* - Correspondence: Yuriy Prylutskyy: prylut@ukr.net, Jacek Piosik: piosik@biotech.ug.edu.pl, Maxim Evstigneev: max_evstigneev@mail.ru

Abstract

A novel nano-formulation of the anticancer drug cisplatin (Cis) with C_{60} fullerene (C_{60}+Cis complex) was developed, demonstrating enhanced cytotoxic activity towards tumor cell lines *in vitro* n comparison to Cis alone. The enhanced proapoptotic activity of the novel complexes was found to be tightly connected with their unique capability to circumvent cancer drug resistance *in vitro*, as revealed by investigation of human leukemia cells HL-60 together with their sublines resistant towards doxorubicin (HL-60/adr, multidrug resistance protein-1=MRP-1=ABCC1 overexpressing) and vincristine (HL-60/vinc, P-glycoprotein=P-gp=ABCB1 overexpressing). The enhanced anticancer activity of the developed C_{60}+Cis complexes was also confirmed *in vivo* on male C57BL/6J mice bearing Lewis lung carcinoma, effectively inhibiting tumor growth and formation of metastases in comparison to free single Cis.

For better understanding of molecular mechanisms underlying the potential ability of the C_{60}+Cis complexes to circumvent cancer drug resistance, a molecular docking study was conducted. This analysis demonstrated the potential capability of C_{60} fullerene to form van der Waals interactions with potential binding sites of P-gp, MRP-1and MRP-2 (ABCC2) molecules, with maximum affinity to MRP-2. The observed phenomenon might indicate the

mechanism how the C_{60}+Cis complex bypasses drug resistance of cancer cells by direct binding to ABC transporter proteins. Additionally, the results of Ames mutagenicity test demonstrated that immobilization of Cis on C_{60} fullerene significantly diminishes mutagenic activity of Cis and may reduce the probability of secondary neoplasms induction.

Concluding, the synthesized C_{60}+Cis complex effectively induces cancer cell death *in vitro* and inhibits tumor growth *in vivo*, circumventing cancer cell resistance to chemotherapy due to the specific affinity of C_{60} fullerene towards ABC-transporter proteins. The obtained results indicate the C_{60}+Cis complex as a promising novel chemotherapeutic agentespecially for treatment of drug-resistant tumors.

Keywords

Molecular docking, small-angle X-ray scattering, apoptosis, mutagenic activity, Lewis lung carcinoma, cytotoxicity

Introduction

Chemotherapy is one of the principal modes of systemic cancer treatment, but its success is often limited due to low selectivity of standard chemotherapeutics (doxorubicin, vincristine, cisplatin) which are also toxic to non-malignant, rapidly dividing cells, thus, causing serious side effects in cancer patients [1]. There are many reasons behind the failure of cancer treatment, but the main one is acquired cancer drug resistance to chemotherapy, caused by over-expression of specific ABC-transporter proteins and/or multiple defects in genes involved in cell cycle and apoptosis regulation in cancer cells [2, 3].

One of the most extensively used anticancer chemotherapeutics is cisplatin (Cis-$[Pt(II)(NH_3)_2Cl_2]$, Cis), a water soluble derivative of inorganic divalent platinum [4]. Cis exerts its anticancer activity by cross-linking the DNA strands and further induction of apoptosis. However, this anticancer activity is accompanied by severe adverse effects as mentioned above [4]. Therefore, development of new alternative methods of Cis delivery towards tumor cells, which allow increasing drug activity in the malignant tissue and its bioavailability within the organism, is of great importance to clinical oncology and pharmacology. This can be realized by application of specific nanoscale carriers of different origin, e.g. by either encapsulation of the platinum-based anticancer drugs in polymeric matrix or their conjugation with the polymeric carrier [5]. It was shown that conjugation of drug with polymeric carrier not only increases its bioavailability but also promotes selective drug transfer to the tumor growth area [6]. Moreover, conjugation of dichloro (1,2-diaminocyclohexane) platinum(II) on nanoparticles coated with hyaluronic acid led not only to increase of its bioavailability, but also to effective circumvention of drug resistance of tumor cells to chemotherapy [7]. Therefore, novel nanocarriers should not only significantly lower the negative side effects of specific chemotherapeutic agents, but also enhance their anticancer activity [8, 9].

In this work we propose C_{60} fullerene (FC_{60}) as a promising platform for the delivery of Cis and other drugs. FC_{60} is a carbon nanostructure reported to possess biological activity towards various types of cells both *in vitro* and *in vivo* [10]. Pristine FC_{60} is shown to be non-toxic at low concentrations [11-13], penetrate through cell plasma membrane [14-16], and exhibit antioxidant activity [17, 18]. Moreover, FC_{60} possesses its own anticancer activity, suppressing growth of Lewis lung carcinoma on C57BL/6J male mice in 25 mg/kg dose [19,

20]. Proposed mechanisms of FC_{60} antitumor activity are based on its ability to modulate oxidative stress, inhibit angiogenesis and stimulate immune responses [21-25].

Recently we have demonstrated that anticancer drugs with anaromatic core may form non-covalent complexes with FC_{60} in physiological solution [26, 27], which was suggested to be a key process leading to amplification of the antitumor effect of antibiotic doxorubicin (Dox) *in vitro* towards various tumor lines and *in vivo* towards C57BL/6J male mice bearing Lewis lung carcinoma [28-30]. Based on these results, we hypothesized that the anticancer effects of other drugs may also be enhanced by their immobilization on FC_{60} [27, 31], and selected Cis as a potential candidate for conjugation on this novel nanocarrier. It was revealed by us that Cis, like Dox, also forms a non-covalent complex with FC_{60} in the physiological solution [32], which suggests suitability for similar improvement of its anticancer activity *in vitro* and *in vivo*.

Thus, the main goal of current study was to dissect in more detail the mechanisms underlying the antineoplastic potential of novel C_{60}+Cis conjugates with special attention to their ability to bind to ABC transporter proteins *in silico,* circumvent tumor drug resistance and decrease Cis genotoxicity *in vitro*. Finally, therapeutic activity of C_{60}+Cis complexes was evaluated *in vivo* on the Lewis lung carcinoma model in mice.

1. Results and discussion

The low selectivity of conventional anticancer drugs for malignant cells leading to adverse effects [1, 33-36] as well as rapid development of the tumor drug resistance [2, 3] are considered to be two major problems of current cancer chemotherapy.

For addressing these impediments, novel complex of the classical and highly active anticancer drug Cis with FC_{60} was prepared and analyzed. Previous studies on FC_{60} demonstrated its good biocompatibility and potential suitability to be used as delivery platform for another golden chemotherapy standard – namely Dox [29, 30].

1.1. Small-angle X-ray scattering data

First, formation of the complex between Cis and FC_{60} (C_{60}+Cis complex) in the mixture of Cis and FC_{60} using small-angle X-ray scattering (SAXS) was assessed. The experimental SAXS curves of FC_{60} and FC_{60}-Cis aqueous solutions are presented in Figure 1. Processing of the SAXS curves using the approach developed by Glatter [37], based on indirect Fourier transformation, enabled us to calculate the pair distance distribution function for the investigated systems (Figure 1). It should be stressed that the shapes of these functions for FC_{60} and C_{60}+Cis complex are distinctly different with only one maximum observed for FC_{60} alone and two maxima for the complex. According to Glatter [38], the observed phenomenon may be the consequence of the C_{60}+Cis complex formation. Maxima observed for FC_{60}-Cis the solution corresponded to two different entities formed in the solution: FC_{60} clusters and C_{60}+Cis complexes (SAXS analysis of Cis solution does not result in the scattering above 10 nm, data not shown). These data are in agreement with the results previously obtained by us using UV-Vis and small-angle neutron scattering for a similar mixture of FC_{60} and Cis [32]. Due to the fact that SAXS and small-angle neutron scattering methods are complementary, the results of our studies clearly indicate on specific interaction of FC_{60} and Cis in solution leading to their heterocomplexation in the analyzed mixture.

1.2. Molecular docking

Molecular docking is one of the most extensively used computational tool in the simulations of the biophysical systems, especially in a search for molecular targets of new drugs [39-42]. This methodological approach allows to explore the landscape of the conformational energies that may be adopted by the analyzed protein molecule.

Molecular docking of P-gp (=ABCB1) was conducted in each of the four positions of the potential FC_{60} binding (Figure 2A), basing on the available data [43]: *position 1* – part of the protein located in the extracellular space (Extra-Cell); *position 2* – native binding site of the protein; *position 3* – transmembrane domains (Membrane Interior); *position4* – part of the protein located in the intracellular space (Intra-Cell). The obtained energy characteristics for the FC_{60}+P-gp complex are presented in Table 1.

FC_{60} binding in the *positions 1,2 & 3* is characterized by the complete filling of the binding pockets and low interaction energies between FC_{60} and P-gp (Table 1). However, *position 1* is characterized by significant steric clashes between the interacting structures (19.1 kJ/mol), while, in case of the *positions 2,3 & 4* these values are negligible, reaching values as low as 1.6 kJ/mol for the *position 2* (Table 1). It is noteworthy, that *position 4* is characterized by only a partial filling of the potential binding site and the highest interaction energy (-54 kJ/mol). The energy of hydrogen bonds as well as the energy of FC_{60} steric clashes equal zero for all binding sites.

The following amino acids are involved in the formation and stabilization (van der Waals interactions) of the FC_{60}+P-gp complex (Figure 2A):

- *position 1*: Ile 730, Ile 731, Lys 734,Arg 741, Ile 852, Tyr 853, and Glu 932;
- *position 2*: Tyr 310, Phe 336, Leu 339, Ile 340, Phe 343, Gln 725, Phe 728, Phe 732, Tyr 953, Phe 983, and Met 986;
- *position 3*: Ser 180, Asn 183, Glu 184, Asp 188, Lys 189, Leu 879, Gln 882, Ala 883, and Phe 938;
- *position 4*: Ala 259, Arg 262, and Glu 1119.

The molecular docking of FC_{60} to MRP-1 (=ABCC1) was performed at the native binding site of the protein (Figure 2B). The simulated FC_{60}+MRP-1 complex is characterized by an interaction energy lower than the values obtained for P-glycoprotein in any of the binding sites (-50.7 kJ/mol) and minor steric clashes (5.9 kJ/mol) comparable to those obtained for P-gp in *positions 2,3 & 4*. The amino acids involved in the interactions are: Leu 692, Glu 694, Val 708, Ala 709, Tyr 710, Trp 716, Phe 728, and Arg 780 (Figure 2B).

Finally, the simulated FC_{60}+MRP-2 (=ABCC2) complex was characterized by the following parameters: the energy of interaction between the FC_{60} and protein is -61.5 kJ/mol, the energy of steric clashes between the FC_{60} and protein is 13.6 kJ/mol and, that importantly, in this case the binding pocket is completely filled (Figure 2C). The key interactions occur with Phe 87, Trp 75, Glu 53, Leu 51, Tyr 69, Thr 67 andGln 143.

The results of the molecular docking experiments suggest a direct interaction between FC_{60} and three of the main proteins involved in multidrug resistance phenotypes of cancer cells –namely P-gp, MRP-1 and MRP-2. However, in a report devoted to analysis of interactions of MRP-1 with curcumin *in silico*, other aminoacid residues involved in formation of the protein binding cavity, were proposed [44]. The reason behind these differences may be the diverse modeling method used in this work and by Sreenivasan *et al.* [44]. Additionally, there is a huge difference in the structures of FC_{60} and curcumin. The first

is the large spherical particle, while the latter has two aromatic rings connected by long chain of carbon atoms.

1.3. *In vitro* toxicity

Based on promising results of molecular docking studies, the potential ability of C_{60}+Cis complex to circumvent tumor drug resistance was studied *in vitro* using cell lines with acquired multidrug resistance phenotypes. Several tumor cell lines differing in the drug resistance mechanisms (overexpression of P-gp, MRP-1, knockout of key genes, involved in cell cycle regulation and apoptosis) were addressed which belong to three cancer types commonly treated with Cis, namely colon [45, 46], cervix cancer [47-49] and leukemia [50].

It was revealed that C_{60}+Cis complexes possessed higher cytotoxic activities compared to Cis alone towards human colon cancer cells. However, on HCT-116/wt line and its HCT-116/Bax (-/-) subline (with knocked out Bax gene) the differences in effects of C_{60}+Cis complex and Cis alone were statistically insignificant. Nevertheless, HCT-116/p53 (-/-) cell line (with knocked out p53 gene) was found to be more sensitive (by 20%) to C_{60}+Cis complex at a dose of 5 μM as compared to Cis alone ($p<0.05$) (see Figure 3).

Beneficial effects of Cis complexation with FC_{60} were even more pronounced when analyzed on the human cervix cancer cell lines. In case of HeLa and KB-3-1 cells the cytotoxic activity of the analyzed C_{60}+Cis complex was 20-25% higher than Cis alone. Surprisingly, colchicine-resistant KBC-1 subline (overexpressing P-gp) was hypersensitive to Cis action, but even in this case C_{60}+Cis complex demonstrated 10-15% higher cytotoxicity than Cis alone (Figure 3).

However, the highest difference (over 2-fold) in the cytotoxic activity between the C_{60}+Cis complexes and Cis was observed on human HL-60 leukemia cells and its drug-resistant sublines, characterized by expression of various ABC-transporter proteins. LC_{50} (lethal concentration of drug which kills 50% of tumor cells) of Cis was 0.85 μM for parental HL-60 cells, while for the C_{60}+Cis complex this index was 2.2-fold lower (LC_{50}=0.38 μM). The drug-resistant HL-60/adr subline (MRP-1 overexpression) demonstrated a 20-fold lower sensitivity to Cis (LC_{50}=17.51 μM), while the C_{60}+Cis complex fully preserved its 2.2-fold higher activity (LC_{50}=7.67 μM), as found on wild-type cells. The same tendency was also observed on another multidrug-resistant HL-60 subline, HL-60/vinc cell line (overexpressing P-gp), where the C_{60}+Cis complex (LC_{50}=6.68 μM) displayed even a higher effect (3.3 fold) towards Cis (LC_{50}=21.99 μM). On contrary, human Jurkat T-leukemia cells demonstrated only a little difference in sensitivity against Cis and C_{60}+Cis complex thus indicating that the impact of FC_{60} on the cytotoxic effects of Cis varies from one cell line to another (Figure 4).

Chemotherapy resistance is a central problem for the modern medicine and is drawing increasing attention worldwide [2, 3]. Drug resistance mechanisms analyzed in this work, namely Bax and p53 protein deletions as well as overexpression of drug resistance proteins P-gp and MRP-1, are among the most prominent and widespread factors in clinical therapy failure [51, 52]. Therefore, the development of novel drug delivery systems, able to increase the efficacy of anticancer drugs and to circumvent resistance acquirement remains an extremely important task of modern pharmacology and medicine [7-9]. Reports of numerous groups working on the improvement of Cis therapy have already shown that several compounds possess these unique properties. In particular, Sui *et al.* demonstrated that yet another nanocarbon structure – graphene – also enhances Cis anticancer activity by increasing its uptake to the cell and its nucleus [53], the mechanism also described for FC_{60} [14-16]. Structurally different nanocarriers, such as shikonin [52] or dibenzo[*c,h*][1,6]naphthyridin-6-

one [54] also increased Cis cytotoxicity towards HCT-116 cell line, while Cis complex with benzyl isothiocyanate [55] demonstrated similar effects in the HL-60 cell line. Curcumin [56], cyclooxygenase inhibitors [57], tetrandrine [58] or melatonin [59] were shown to circumvent tumor drug resistance *in vitro*, but none of the aforementioned compounds possessed all desired characteristics (namely, decreasing drug side effects, enhancement of its cytotoxicity, circumvention ofdrug resistance) in contrast to C_{60}+Cis complex, analyzed in this work. Nevertheless, it should be stressed that Cis resistance is a very complex phenomenon involving different factors, e.g. ABC-transporters like MRP-2, ATP7A/ATP7B, status of reduced/oxidized cellular glutathione system and metallothioneins [60]. Besides these proteins, MRP-1 and P-gp also seem to play supporting roles here [61], which was confirmed by our own studies.

1.4. Assessment of the cell cycle and apoptosis

In order to study potential mechanism underlying increased cytotoxic activity of C_{60}+Cis complexes, their impact on apoptosis induction and cell cycling in tumor cells was studied using flow cytometry and fluorescence microscopy. Chromatin condensation is considered a typical apoptotic hallmark, which can be easily measured using DNA-intercalating dyes, such as DAPI. It was revealed that KB-3-1 human cervix carcinoma cells treated with FC_{60} (Figure 5D) were characterized by intact nuclei resembling the control samples (Figure 5A), indicating absence of proapoptotic activities of the nanocarrier itself. Cis alone led to appearance of cells with hypercondensed nuclei and formation into apoptotic bodies (Figure 5B), but its complexation with FC_{60} further enhanced this proapoptotic activity of the anticancer drug (Figure 5E). This phenomenon can be clearly seen due to the massive increase in the percentage of shrinked cells with condensed nuclei. This effect was even more pronounced when the concentrations of the drug and complex were increased to 20 μM (Figure 5C and Figure 5F, respectively).

MRP-1 overexpressing HL-60/adr cells were addressed for confirmation of the obtained results on a drug-resistant cell line. Due to the fact that HL-60/adr cells are leukemia cells and thus cannot be properly stained with DAPI due to small size of their nuclei and their growth in suspension, annexin V/propidium iodide double staining by means of flow cytometry was used here. C_{60}+Cis complex led to a significant increase in the number of annexin V-positive cells compared to single Cis at all used concentrations (10, 15 and 20 μM) (Figure 6A), but the most prominent effect was observed for the 15 μM dose of these compounds (19,16% vs 10,11%, $p<0.01$). Cell cycling studies using propidium iodide staining have revealed that C_{60}+Cis complexes have no impact on redistribution of HL-60/adr cells in $G_1/S/G_2$ phases of cell cycle compared to single CDDP (Figure 6B). However, C_{60}+Cis nanocomposites led to a clear-cut, 2-fold increase of number of pre-G_1 (apoptotic cells) compared to Cis alone, which was observed for all tested drug concentrations ($p<0.05$). These data additionally verify the annexin V/PI and DAPI staining experiments, thus confirming our working hypothesis about the distinctly enhanced proapoptotic activity of the C_{60}+Cis complexes compared to Cis alone towards tumor cells *in vitro*.

Apoptosis is one of the most prominent mechanisms of Cis anticancer activity [4, 62] and proapoptotic potential of the drug against leukemia cell line HL-60 is well documented [50]. This phenomenon is widely used in the attempts to enhance the anticancer potential of Cis with numerous biologically active compounds, such as, amongstothers, shikonin [52] or oridonin [63]. The results of the staining experiments presented in this work also indicate a higher proapoptotic activity of the C_{60}+Cis complex compared to Cis alone. Therefore, they

support the hypothesis that C_{60}+Cis complex possesses higher anticancer activity than the Cis alone due to enhanced induction of apoptosis.

1.5. Ames mutagenicity assay

Ames test on *Salmonella typhimurium* culture was applied for evaluation of the potential mutagenic activity of the C_{60}+Cis complex. It was revealed that administration of Cis together with the FC_{60} led to significant reduction of Cis mutagenic activity (Figure 7). However, this reduction was not dependent on the FC_{60} dose, since a protective effect was comparable at all concentrations of FC_{60} except the lowest (10 ng/plate) which corresponds to C_{60}:Cis molar ratio of 1:120. When this ratio was lowered to 1:24, the observed protective effect did not statistically change as compared to one observed at the highest FC_{60} concentration used (10 μg/plate; C_{60}:Cis molar ratio 1:8.3). The highest protective effect was observed for a C_{60}:Cis molar ratio of 1:2 (corresponds to 0.6 μg/plate). This phenomenon can be attributed to an increased homo-aggregation of the FC_{60} at high concentration, which may reduce a number of binding sites available for Cis. Consequently, this may lead to an increased number of unbound Cis in biologically active form. Nevertheless, an observed reduction of Cis mutagenic activity by lower concentrations of the FC_{60} showed a pattern similar to one detected for other compounds with a confirmed mutagenic activity, such as ICR-191 [64], the heterocyclic aromatic amines [65, 66] or anticancer drugs [67, 68]. It should be stressed that the observed optimal C_{60}:Cis molar ratio of 1:2 on Ames test is almost identical to the molar ratio of C_{60}:Cis used for the *in vitro* studies on tumor cell lines (1:2.4). This was obtained by mixing 500 μg/ml solutions of Cis and FC_{60}. Other molar ratios of FC_{60} and Cis (namely 1:0.6, 1:1.2 and 1:4.8) have proven to be less effective compared to the studied C_{60}+Cis complex (see Supp. Figure 1).

1.6. Antitumor action *in vivo*

Lewis lung carcinoma (LLC) is widely used as an experimental murine tumor model for evaluation of the efficiency of novel anticancer therapies [8, 29, 69-74]. Consequently, we used this well-established tumor model to test our novel drug formulations as well. All treatment (namely FC_{60}, Cis and C_{60}+Cis complex) resulted in a decrease in the tumor volume, when compared to the *control* (untreated group) (Figure 8). At the 20^{th} day of the experiment the tumor volume in mice of *group 1* (treated with FC_{60}) and *group 2* (treated with Cis alone) was 15% reduced as compared to the *control*. The most prominent antitumor effect, however, was observed in case of the mice in *group 3* (treated with C_{60}+Cis complex), where the decrease in the tumor volume reached 75% of the *control* (Figure 8).

At the next step of our studies, tumor growth inhibition index (TGII) was calculated (see Table 2). The value of TGII in *group 1* was increasing between day 11^{th} and 17^{th}, however on the 20^{th} day of the experiment it decreased rapidly (from 35% to 17%). Even a higher decrease in the TGII value was observed in case of the *group 2* (48% to 18% between 17^{th} and 20^{th} day). Despite reduction (52% to 36%) of TGII in the last period of the experiment for *group 3* (treated with C_{60}+Cis complex), the final value was still twice as high as the values observed for the groups treated with either FC_{60} or Cis alone. This indicates that the inhibitory effects of the C_{60}+Cis complex on the growth of the LLC model are more pronounced and longer lasting than its components alone.

LLC is characterized by high metastasis to the lungs [75, 76]. Therefore, at the time of experiment cessation (22^{nd} day) the number of metastatic nodules on the surface of each lung

lobule of every mouse as well as their volume were evaluated. All analyzed therapies reduced both the total volume of lung metastases and the average volume of the single metastasis. However, the average number of the metastases in the mice treated with Cis alone was comparable to the *control* (12 to 13, respectively). In case of groups treated with either FC_{60} or Cis the reduction of the total metastases volume reached 73% and 57%, while the volume of the single metastasis was decreased by 50% and 53%, respectively. However, the most pronounced decrease of all analyzed parameters was observed in *group 3,* where the total metastases volume was reduced by 75% and the volume of the single metastasis by 64% compared to the control group.

Another well described characteristic of LLC bearing mice is tumor associated cachexia [77, 78]. It was revealed that body weight of animals after tumor removal in the untreated *control* group was 28% lower compared to *intact animals* group (mice not bearing LLC). Interestingly, body weight of mice treated with Cis alone (*group 2*) was lower than in the *control* by 10% what resulted in overall weight loss equal to 35% of the weight of healthy animals. Animals treated either with FC_{60} (*group 1*) or C_{60}+Cis complex (*group 3*) had a body weight significantly lower than *intact animals*, however, the loss of body mass was reduced and only reached 22% and 15%, respectively.

The main triggering factors of cancer cachexia are systemic inflammation and disorders in the lipid metabolism [79]. One of the most extensively studied properties of FC_{60} is its potential to scavenge free radicals [17, 18, 23, 24]. Therefore, it might be hypothesized that the reduced manifestation of cancer cachexia in animals treated with FC_{60} alone or C_{60}+Cis complex might be associated with this ability of FC_{60}.

Interestingly, increasing number of studies report that cytotoxic anticancer drugs, including Cis, besides promoting apoptosis [3, 4, 80], may act as modulators of immunological activity [81-84]. Moreover, carbon nanostructures are reported to possess immunomodulatory activity as well [25]. Therefore, we evaluated the response of the immune system of tumor-bearing mice to chemotherapy treatment by calculating thymus and spleen weight indices. All proposed treatments resulted in a significant decrease in the splenic index as compared to the *control*. However, the observed values were still 28-44% higher compared to the ones in the *intact animals*. Interestingly, thymic index value calculated for untreated animals was comparable to healthy animals while every treatment resulted in the decrease of the thymus weight (Table 5).

It is known that progression of LLC is accompanied with moderate splenomegaly – manifestation of a hematological paraneoplastic syndrome [85]. The weight of the spleen of mice undergoing any treatment (including C_{60}+Cis complex) was significantly lower than in the *control* (untreated) group of LLC bearing mice. This phenomenon was also observed in case of the splenic indices, however, the values calculated for mice treated with Cis alone (*group 2*) were relatively higher than the values obtained for groups treated with FC_{60} and C_{60}+Cis complex. We can hypothesize that this relative decrease in the thymus weight may be the result of an increase of thymocyte apoptosis, a decrease in thymocyte proliferation or an increase in the translocation of thymocytes from the organ to periphery. Numerous reports indicate internalization of FC_{60} by the murine dendritic cells [86-88]. Additionally, the authors suggest that these nanoparticles may be recognized by Toll-like receptors and, therefore, stimulate the major histocompatibility complex class I – restricted T-cell response associated with thymocyte migration to periphery [86-88]. Considering these literature reports and our results, we hypothesize that FC_{60}-induced activation of the cell-mediated immune

response can be one of potential causes of a decrease in the thymus weight in mice treated with either FC_{60} or the C_{60}+Cis complex.

2. Conclusions

The biological activity of novel Cis nanoformulations based on C_{60} fullerene was studied *in vitro* and *in vivo*. Complexation of Cis with FC_{60} increases the cytotoxic activity of the drug *in vitro* towards tumor cell lines with various mechanisms of drug resistance, which may be explained by the increased proapoptotic potential of C_{60}+Cis complex, as revealed by fluorescence microscopy and flow cytometry studies. In turn, effective circumvention of tumor drug resistance by C_{60}+Cis complex may be caused by specific binding of FC_{60} to several ATP-binding cassette transporters involved in the efflux of anticancer drugs, as revealed by molecular docking studies, leading to their inactivation. It should be stressed that MRP-2, which is considered the main ABC-transporter involved in resistance of tumor cells to Cis [60], was also found to possess the highest affinity to FC_{60}, thus confirming our hypothesis.

The enhanced cytotoxic activity of C_{60}+Cis complexes *in vitro* was also confirmed using *in vivo* studies on C57BL/6J male mice bearing Lewis lung carcinoma. Treatment with C_{60}+Cis complex resulted in a 2-fold increase of the tumor growth inhibition index compared to free Cis and FC_{60}, applied alone. Moreover, metastases in mice treated with the C_{60}+Cis complex were characterized by the lowest total volume and average size. This enhanced activity is associated with reduction of tumor-associated splenomegaly as well as decrease of the thymus weight by FC_{60}. Additionally, the observed decrease inmutagenic activity of Cis in the complex with FC_{60} implicates a decreased risk for the probability to develop secondary neoplasms induced by Cis.

In summary, the data obtained in this study support our initial hypothesis concerning a synergism in the biological activities of FC_{60} and Cis associated with their ability to form non-covalent complexes in the physiological conditions. Moreover, our results suggest that the C_{60}+Cis complex may be a promising candidate for the development of novel regimens for treatment of drug-resistant tumors.

3. Methods

3.1. Materials preparation

3.1.1. Preparation of C_{60} fullerene aqueous colloid solution

The pristine FC_{60} aqueous colloid solution (maximal concentration 0.5 mg/ml) used in the experiments was prepared according to the protocols developed before [89, 90].

3.1.2. Preparation of Cis complex with C_{60} fullerene

Cis solution (Cisplatin-TEVA, Pharmachemie B.V., 0.5 mg/ml) was immobilized on the FC_{60} according to the protocol developed by our research group [32]. The initial solution of Cis and FC_{60} aqueous solution were mixed in 1:1 volume ratio. Afterwards the mixture was treated for 20 min in ultrasonic disperser and underwent overnight magnetic stirring at room temperature.

3.2. Small angle X-ray scattering measurements

SAXS experiments were performed at the P12 BioSAXS Beamlineat PETRA III ring (EMBL/DESY) using the 100 (V) µM x 200 (H) µm X-ray beam and energy 10 keV. The sample to detector distance, 3.1 m, resulted in the q-range 0.07-4.6 nm^{-1} after calibration using silver behenate [91]. Scattering patterns were recorded by a Pilatus 2M pixel detector. The samples (20 µL) were injected into the sample capillar using an automated sample changer. The sample was moved during the exposure to reduce the risk of the radiation damage. Twenty consecutive frames (0.05 s) containing sample and buffer measurements were performed at the 20 °C. All scattering curves of the recorded dataset were compared to the reference measurement (typically the first exposure) to exclude any artefacts, and then integrated by automated acquisition program [92]. Signal of pure buffer was measured pre- and post- sample measurement and used for background subtraction. All data were normalized to the transmitted beam and processed using indirect Fourier transformation approach developed by Glatter [37] and applying GNOM program [93].

3.3. Molecular docking

3.3.1. P-glycoprotein (P-gp)

Protein data banks PDB, PDBe and pfam contain only murine P-gp structure. Therefore, as presented study was conducted on human tumor cell lines, all attainable P-gp structures were compared with each other using ClustalW software. The most representative structure 4M1M was selected [94] and further used as a template for construction of a human P-gp model, which was built on Swiss-Model online server (www.expasy.ch/swissmod).

3.3.2. Multidrug resistance protein 1 (MRP-1)

All attainable structures of MRP-1 in ClustalW software and the most representative structure 2CBZ were selected [95].

3.3.3. Multidrug resistance protein 2 (MRP-2)

Due to the fact that PDB contains the structure of MRP-2 for Plasmodium yoelii (PDBID 2GHI (Crystal Structure of Plasmodium yoelii Multidrug resistance protein 2) [96], we conducted a homologous simulation of MRP-2 structure to the human organism. The amino acid sequence of MRP-2 was obtained from the UniProt, ID sequence Q92887. In the process of comparison it was found that it is less similar to the 2GHI structure (identity - 30.6%, similarity - 44.3%) than to the 2CBZ structure (identity - 60.6%, similarity - 70.6%; this structure was used for modeling of FC_{60}+MRP-1 complex). In addition, upon imposing 2CBZ on 2GHI it was revealed that all secondary structures were overlapping. Given this, the 2CBZ structure [95] was used as the template for the homologous modeling of MRP-2 structure to the human organism.

3.3.4. Molecular docking simulation

Water molecules were removed from the selected proteins and Arg and Lys residues were protonated. The procedure was performed using the flexible ligand model employing systematic docking algorithm (sdock+) [96]. 100 calculations steps were performed for each protein and 10 best FC_{60}-protein complexes (basing on QXP scoring functions [97]) were further analyzed. The mobility range of all of interacting structures, from small side chains to large-scale domain movements was considered throughout the calculations. Following energy types were evaluated: ***FreE*** – the energy of complex; ***Cntc*** – the energy of interactions

between the FC_{60} and protein; ***Bump*** – the energy of steric clashes between the FC_{60} and protein.

3.4. Cytotoxicity studies

Human isogenic p53-null (p53-/-), Bax-null (Bax-/-), and wild-type (p53+/+, Bax+/+) HCT-116 colon carcinoma cell lines were kindly provided by Dr. Bert Vogelstein, John Hopkins University, Baltimore, USA. The human HeLa cervix cancer cell line and the human Jurkat T-leukemia cell line were derived from ATCC. The human cervix carcinoma KB-3-1cell line and its colchicine-selected KBC-1 subline (P-gp overexpressing) were a generous gift from Dr. Shen, Bethesda, USA [98]. The human leukemia HL-60 cell line and its drug-resistant sublines Hl-60/adr (overexpressing of MRP-1) and HL-60/vinc (P-gp overexpressing) were donated by Dr. M. Center, Kansas State University, Manhattan, KS. [99].

Cells were cultured in RPMI-1640 medium (Sigma-Aldrich, St. Louis, USA) supplemented with 10% fetal calf serum (Sigma-Aldrich, St. Louis, USA), 50 μg/ml streptomycin (Sigma-Aldrich, St. Louis, USA), and 50 units/ml penicillin (Sigma-Aldrich, St. Louis, USA) in 5% CO_2 humidified atmosphere at 37 °C. During experiments, cells were incubated for 24 h in 24-wells tissue culture plates (Greiner Bio-one, Frickenhausen, Germany) and the cytotoxic effects of Cis and C_{60}+Cis complex were evaluated under Evolution 300 Trino microscope (Delta Optical, NoweOsiny, Poland) by staining the dead cells with trypan blue dye (0.1%).

3.5. Chromatin condensation test

Human cervix carcinoma KB-3-1 cells treated with FC_{60}, Cis, and the C_{60}+Cis complex were stained with DAPI (4',6-diamidino-2-phenylindole, Sigma Aldrich, St. Louis, USA) for analysis of nuclear chromatin condensation. After 24 h drug incubation, cells were washed twice with PBS, fixed in 4% solution of paraformaldehyde for 15 min at the room temperature, and permeabilized with 0.1% Triton X-100 in the PBS buffer for 3 min. Subsequently, cells were incubated with 1 μg/ml DAPI solution for 5 min, washed twice with PBS, and cover glasses with fixed cells were placed on slides. Cytomorphological studies were performed using Carl Zeiss AxioImager A1 fluorescent microscope (Carl Zeiss, Gottingen, Germany).

3.6. Apoptosis analysis

For cell death analyses, cells were stained with annexin-V-FITC and propidium iodide (PI) using an apoptosis detection kit (BD Biosciences, San Jose, CA), according to the manufacturer's instructions. In particular, 24 h after the addition of various concentration of FC_{60}, Cis and C_{60}+Cis complex, HL-60/adr cells were centrifuged at 2,000 rpm, washed twice with 1x PBS, and incubated for 15 min in Annexin V binding buffer (BD Pharmingen, USA) containing 1/50 volume of FITC-conjugated Annexin V solution and PI (50 μg/ml). Then samples were diluted 2 times by appropriate volume of Annexin V binding buffer (BD Pharmingen, USA) and immediately measured on FL1/FL2 (FITC-PI) channels of FACScan flow cytometer (Becton Dickinson, USA).

3.7. Cell cycle analysis

Cell cycle distribution of the analyzed cell cultures was assessed according to protocol described by Walker *et al.* [100]. After drug treatment, 2×10^6 cells HL-60/adr cells collected, pelleted by spinning at 1,000 rpm, 4 °C for 5 min, resuspended in 1 ml of cold PBS and fixed by adding dropwise 4 ml of -20 °C absolute ethanol. On the next day, fixed cells were centrifuged again and cell pellets were resuspended in 1 ml of PBS. Then 100 µl of 200 µg/ml DNase-free RNaseA (Invitrogen, USA) were added to cell suspension and incubated at 37 °C for 30 min. After this, 100 µl of 1 mg/ml propidium iodide was added to samples, which were incubated at room temperature for 5-10 min and then analyzed on FACScan flow cytometer (Becton Dickinson, USA). Cell cycle analysis was carried out using the Cytomation Summit Software v3.1 (CytomationInc, USA).

3.8. Ames mutagenicity test

The *Salmonella typhimurium* TA102 strain used in Ames mutagenicity test was kindly provided by Prof. H. Czeczot from Department of Biochemistry, Medical University of Warsaw (Poland). Ampicillin, histidine and biotin were purchased from Sigma Aldrich Chemical Company (St. Louis, USA).

The *Salmonella* mutagenicity test was performed using *Salmonella typhimurium* TA102 strain – without metabolic activation according to the procedure described by Mortelmans and Zeiger [101] with modifications introduced by Woziwodzka *et al.* [66].

A mixture containing 100 µL of overnight culture of *S. typhimurium* TA102 (corresponding to 1×10^8 colony forming units), 50 µL of 3% NaCl and 100 µL of test chemicals dilution (or sterile water for the negative control) was incubated for 4 h in darkness at 37 °C and 220 rpm. Afterwards, the mixture was centrifuged, bacterial pellets washed with 0.75% NaCl and resuspended in 300 µL of 0.75% NaCl solution containing 0.1 µmol histidine and 0.1 µmol biotin. Finally, it was spread on glucose minimal (GM) plate. All experiments were performed in triplicate. After 48 h incubation at 37 °C in darkness, the number of revertant colonies was calculated. The possible bacterial toxicity was determined by observation of the auxotrophic background (background lawn). Analyzed FC_{60} concentration was proven to be non-toxic towards *S. typhimurium* TA102, as no alterations in the background lawn were observed.

3.9. *In vivo* procedures

Male mice (weight 18-19 g) of C57BL/6J line were bred and maintained on a standard diet at 25±1 °C in the animal facility of R.E. Kavetsky Institute of Experimental Pathology, Oncology and Radiobiology, NAS of Ukraine (Kyiv, Ukraine). All experiments were conducted in accordance with the international regulations of the European Convention for protection of vertebrate animals under control of the Bio-Ethical Committee of the NAS of Ukraine.

LLC cells were kindly provided by the National Bank of Cell Lines and Transplanted Tumors at R.E. Kavetsky Institute of Experimental Pathology, Oncology and Radiobiology, NAS of Ukraine. The mice were randomized by weight and divided into 5 groups (10 animals per group). Four of them received transplantation of 3×10^5 of the tumor cells into the limb via intramuscular injection. These groups were intraperitoneally injected with: saline (*control group*), FC_{60} (*group 1*) and Cis (*group2*) at a dose of 1.25 mg per kg body mass, and C_{60}+Cis complex (*group 3*) at a dose of 2.5 mg per kg body mass. The remaining, fifth group of mice

did not undergo tumor transplantation (*intact animals*). Injections of the analyzed substances were conducted every other day for a total period of 10 days, with the first injection on the 2nd day after tumor transplantation. The protocol of FC_{60} administration and the applied dose were established on the basis of experiments described previously [17].

Kinetics of LLC tumor growth in mice was characterized by observation of a change in the tumor size from the 11th day (visual observation, increase of the tumor volume) up to the 20th day. On the 22nd day (first death in the *control* group) mice from all groups were sacrificed by cervical dislocation and autopsied to calculate the number of lung metastases. Every mice from each group, as well as their organs (namely thymus, liver, and spleen) were weighted.

Antitumor efficacy of the proposed treatment was estimated by following indicators [19, 22]:

- tumor volume (V, mm^3)

$$V = \frac{1}{2}\left(\frac{a+b}{2}\right)^3 , \quad (1)$$

where ***a*** and ***b*** are the long and short diameters of the tumor (mm), respectively;

- tumor growth inhibition index (*TGII*, %)

$$TGII = \frac{V_C - V_{Exp}}{V_C} \cdot 100\% , \quad (2)$$

where $\boldsymbol{V_C}$ and $\boldsymbol{V_{Exp}}$ are the average tumor volumes in animals in the control and experimental groups, respectively;

- metastasis volume (V_M, mm^3)

$$V_M = \frac{\pi d^3}{6} , \quad (3)$$

where ***d*** is the linear size of the metastatic nodule (mm);

- thymus and spleen indices

$$k = \frac{m_O}{m} \cdot 1000 , \quad (4)$$

where $\boldsymbol{m_O}$ and ***m*** are weight of the animal's organ (g) and body, (g) respectively.

3.10. Statistical analysis

All experiments were performed in triplicate, and their results were evaluated statistically using Student's *t*-test. The results of the Ames test were evaluated statistically using Statistica 9.1 (StatSoft) software. One-way analysis of variance (ANOVA) followed by the post-hoc Tuckey's HSD test was applied. Significance level was established at $\alpha=0.05$.

Acknowledgements
We gratefully acknowledge the technical support from Clement Blanchet (EMBL) at the P12 BioSAXS beamline (EMBL/DESY, PETRA III). These studies were partially supported by

Russian Science Fund (project No. 14-14-00328), personal WUMBRC grant, given to R. Panchuk, and personal grant of Platon Kostyuk Foundation, given to S. Prylutska.

Reference List

[1] Corrie, P. G. Cytotoxic chemotherapy: clinical aspects. *Medicine* **2008**, *36*, 24-28.

[2] De Vita, V. T.; Lawrence, T. S.; Rosenberg, S. A. *Cancer: principles & practice of oncology: primer of the molecular biology of cancer*; Lippincott Williams & Wilkins, 2012.

[3] Hirsch, J. An anniversary for cancer chemotherapy. *Jama* **2006**, *296*, 1518-1520.

[4] Florea, A.-M.; Büsselberg, D. Cisplatin as an anti-tumor drug: cellular mechanisms of activity, drug resistance and induced side effects. *Cancers* **2011**, *3*, 1351-1371.

[5] Huynh, V. T.; Scarano, W.; Stenzel, M. H. Drug delivery systems for platinum drugs. *Nanopharmaceutics: The Potential Application of Nanomaterials* **2013**, 201.

[6] Carmona, R.; Liang, X.-J. Improving Platinum Efficiency: Nanoformulations. In *Nanopharmaceutics: The Potential Application of Nanomaterials*. World Scientific, 2013; pp 243-274.

[7] Liu, L.; Ye, Q.; Lu, M.; Lo, Y.-C.; Hsu, Y.-H.; Wei, M.-C.; Chen, Y.-H.; Lo, S.-C.; Wang, S.-J.; Bain, D. J. A new approach to reduce toxicities and to improve bioavailabilities of platinum-containing anti-cancer nanodrugs. *Scientific Rports* **2015**, *5*, 10881.

[8] Dong, X.-P.; Xiao, T.-H.; Dong, H.; Jiang, N.; Zhao, X.-G. Endostar combined with cisplatin inhibits tumor growth and lymphatic metastasis of lewis lung carcinoma xenografts in mice. *Asian Pacific Journal of Cancer Prevention* **2013**, *14*, 3079-3083.

[9] Yu, H.; Tang, Z.; Li, M.; Song, W.; Zhang, D.; Zhang, Y.; Yang, Y.; Sun, H.; Deng, M.; Chen, X. Cisplatin loaded poly (L-glutamic acid)-g-methoxy poly (ethylene glycol) complex nanoparticles for potential cancer therapy: preparation, in vitro and in vivo evaluation. *Journal of Biomedical Nanotechnology* **2016**, *12*, 69-78.

[10] Cataldo, F.; Da Ros, T. *Medicinal chemistry and pharmacological potential of fullerenes and carbon nanotubes*; Springer Science & Business Media, **2008**.

[11] Andrievsky, G.; Klochkov, V.; Derevyanchenko, L. Is the C_{60} fullerene molecule toxic?! *Fullerenes, Nanotubes, and Carbon Nanostructures* **2005**, *13*, 363-376.

[12] Prylutska, S. V.; Matyshevska, O. P.; Golub, A. A.; Prylutskyy, Y. I.; Potebnya, G. P.; Ritter, U.; Scharff, P. Study of C_{60} fullerenes and C_{60}-containing composites cytotoxicity in vitro. *Materials Science and Engineering: C* **2007**, *27*, 1121-1124.

[13] Johnston, H. J.; Hutchison, G. R.; Christensen, F. M.; Aschberger, K.; Stone, V. The biological mechanisms and physicochemical characteristics responsible for driving fullerene toxicity. *Toxicological Sciences* **2010**, *114*, 162-182.

[14] Prylutska, S.; Bilyy, R.; Overchuk, M.; Bychko, A.; Andreichenko, K.; Stoika, R.; Rybalchenko, V.; Prylutskyy, Y.; Tsierkezos, N.; Ritter, U. Water-soluble pristine fullerenes C_{60} increase the specific conductivity and capacity of lipid model membrane and form the channels in cellular plasma membrane. *Journal of Biomedical Nanotechnology* **2012**, *8*, 522-527.

[15] Bedrov, D.; Smith, G. D.; Davande, H.; Li, L. Passive transport of C_{60} fullerenes through a lipid membrane: a molecular dynamics simulation study. *The Journal of Physical Chemistry B* **2008**, *112*, 2078-2084.

[16] Qiao, R.; Roberts, A. P.; Mount, A. S.; Klaine, S. J.; Ke, P. C. Translocation of C_{60} and its derivatives across a lipid bilayer. *Nano Letters* **2007**, *7*, 614-619.

[17] Gharbi, N.; Pressac, M.; Hadchouel, M.; Szwarc, H.; Wilson, S. R.; Moussa, F. [60] fullerene is a powerful antioxidant *in vivo* with no acute or subacute toxicity. *Nano Letters* **2005**, *5*, 2578-2585.

[18] Prylutska, S.; Grynyuk, I.; Matyshevska, O.; Prylutskyy, Y. I.; Ritter, U.; Scharff, P. Anti-oxidant properties of C_{60} fullerenes *in vitro*. *Fullerenes, Nanotubes and Carbon Nanostructures* **2008**, *16*, 698-705.

[19] Prylutska, S.; Burlaka, A.; Klymenko, P.; Grynyuk, I.; Prylutskyy, Y. I.; Schütze, C.; Ritter, U. Using water-soluble C_{60} fullerenes in anticancer therapy. *Cancer Nanotechnology* **2011**, *2*, 105-110.

[20] Prylutska, S.; Burlaka, A.; Prylutskyy, Y. I.; Ritter, U.; Scharff, P. Pristine C_{60} fullerenes inhibit the rate of tumor growth and metastasis. *Experimental Oncology* **2011**, *33*, 162.

[21] Chen, Z.; Ma, L.; Liu, Y.; Chen, C. Applications of functionalized fullerenes in tumor theranostics. *Theranostics* **2012**, *2*, 238-250.

[22] Didenko, G.; Prylutska, S.; Kichmarenko, Y.; Potebnya, G.; Prylutskyy, Y.; Slobodyanik, N.; Ritter, U.; Scharff, P. Evaluation of the antitumor immune response to C_{60} fullerene. *Materialwissenschaft und Werkstofftechnik* **2013**, *44*, 124-128.

[23] Kato, S.; Aoshima, H.; Saitoh, Y.; Miwa, N. Fullerene-C_{60} derivatives prevent UV-irradiation/TiO2-induced cytotoxicity on keratinocytes and 3D-skin tissues through antioxidant actions. *Journal of Nanoscience and Nanotechnology* **2014**, *14*, 3285-3291.

[24] Bozdaganyan, M. E.; Orekhov, P. S.; Shaytan, A. K.; Shaitan, K. V. Comparative computational study of interaction of C_{60} fullerene and Tris-malonyl-C_{60}-fullerene isomers with lipid bilayer: relation to their antioxidant effect. *PloS One* **2014**, *9*, e102487.

[25] Zhu, J.; Ji, Z.; Wang, J.; Sun, R.; Zhang, X.; Gao, Y.; Sun, H.; Liu, Y.; Wang, Z.; Li, A. Tumor-Inhibitory effect and immunomodulatory activity of Fullerol $C_{60}(OH)_x$. *Small* **2008**, *4*, 1168-1175.

[26] Evstigneev, M. P.; Buchelnikov, A. S.; Voronin, D. P.; Rubin, Y. V.; Belous, L. F.; Prylutskyy, Y. I.; Ritter, U. Complexation of C_{60} fullerene with aromatic drugs. *ChemPhysChem* **2013**, *14*, 568-578.

[27] Prylutskyy, Y. I.; Evstigneev, M.; Pashkova, I.; Wyrzykowski, D.; Woziwodzka, A.; Gołuński, G.; Piosik, J.; Cherepanov, V.; Ritter, U. Characterization of C_{60} fullerene complexation with antibiotic doxorubicin. *Physical Chemistry Chemical Physics* **2014**, *16*, 23164-23172.

[28] Prylutska, S. V.; Didenko, G. V.; Potebnya, G. P.; Bogutska, K. I.; Prylutskyy, Y. I.; Ritter, U.; Scharff, P. Toxic effect of C_{60} fullerene-doxorubicin complex towards tumor and normal cells in vitro. *Biopolymers & Cell* **2014**, *30*.

[29] Panchuk, R.; Prylutska, S.; Chumak, V.; Skorokhyd, N.; Lehka, L.; Evstigneev, M.; Prylutskyy, Y. I.; Berger, W.; Heffeter, P.; Scharff, P. Application of C_{60} fullerene-doxorubicin complex for tumor cell treatment *in vitro* and *in vivo*. *Journal of Biomedical Nanotechnology* **2015**, *11*, 1139-1152.

[30] Prylutska, S. V.; Skivka, L. M.; Didenko, G. V.; Prylutskyy, Y. I.; Evstigneev, M. P.; Potebnya, G. P.; Panchuk, R. R.; Stoika, R. S.; Ritter, U.; Scharff, P. Complex of C_{60} fullerene with doxorubicin as a promising agent in antitumor therapy. *Nanoscale Research Letters* **2015**, *10*, 1.

[31] Prylutskyy, Y. I.; Evstigneev, M.; Cherepanov, V.; Kyzyma, O.; Bulavin, L.; Davidenko, N.; Scharff, P. Structural organization of C_{60} fullerene, doxorubicin, and their complex in physiological solution as promising antitumor agents. *Journal of Nanoparticle Research* **2015**, *17*, 1-9.

[32] Prylutskyy, Y. I.; Cherepanov, V.; Evstigneev, M.; Kyzyma, O.; Petrenko, V.; Styopkin, V.; Bulavin, L.; Davidenko, N.; Wyrzykowski, D.; Woziwodzka, A. Structural self-organization of C_{60} and cisplatin in physiological solution. *Physical Chemistry Chemical Physics* **2015**, *17*, 26084-26092.

[33] Levi, J.; Aroney, R.; Dalley, D. Haemolytic anaemia after cisplatin treatment. *Br Med J (Clin Res Ed)* **1981**, *282*, 2003-2004.

[34] Aguilar-Markulis, N. V.; Beckley, S.; Priore, R.; Mettlin, C. Auditory toxicity effects of long-term cis-dichlorodiammineplatinum II therapy in genitourinary cancer patients. *Journal of Surgical Oncology* **1981**, *16*, 111-123.

[35] Zhou, W.; Kavelaars, A.; Heijnen, C. J. Metformin Prevents Cisplatin-Induced Cognitive Impairment and Brain Damage in Mice. *PloS One* **2016**, *11*, e0151890.

[36] Perobelli, J. Effects of anticancer drugs in reproductive parameters of juvenile male animals and role of protective agents. *Anti-cancer agents in medicinal chemistry* **2016**.
[37] Glatter, O. A new method for the evaluation of small-angle scattering data. *Journal of Applied Crystallography* **1977**, *10*, 415-421.
[38] Glatter, O. The interpretation of real-space information from small-angle scattering experiments. *Journal of Applied Crystallography* **1979**, *12*, 166-175.
[39] Gao, J.; Wang, T.; Qiu, S.; Zhu, Y.; Liang, L.; Zheng, Y. Structure-Based Drug Design of Small Molecule Peptide Deformylase Inhibitors to Treat Cancer. *Molecules* **2016**, *21*, 396.
[40] Fukunishi, Y.; Mashimo, T.; Misoo, K.; Wakabayashi, Y.; Miyaki, T.; Ohta, S.; Nakamura, M.; Ikeda, K. Miscellaneous topics in computer-aided drug design: Synthetic accessibility and GPU computing, and other topics. *Current Pharmaceutical Design* **2016**.
[41] Pandey, R. K.; Kumbhar, B. V.; Sundar, S.; Kunwar, A.; Prajapati, V. K. Structure-based virtual screening, molecular docking, ADMET and molecular simulations to develop benzoxaborole analogs as potential inhibitor against Leishmania donovani trypanothione reductase. *Journal of Receptors and Signal Transduction* **2016**, 1-11.
[42] Andreichenko, K.; Prylutska, S.; Medynska, K.; Bogutska, K.; Nurishchenko, N.; Prylutskyy, Y. I.; Ritter, U.; Scharff, P. Effect of fullerene C_{60} on ATPase activity and superprecipitation of skeletal muscle actomyosin. *Ukrainian Biochemical Journal* **2013**, 20-26.
[43] Xu, X.; Li, R.; Ma, M.; Wang, X.; Wang, Y.; Zou, H. Multidrug resistance protein P-glycoprotein does not recognize nanoparticle C_{60}: experiment and modeling. *Soft Matter* **2012**, *8*, 2915-2923.
[44] Sreenivasan, S.; Ravichandran, S.; Vetrivel, U.; Krishnakumar, S. *In vitro* and *In silico* studies on inhibitory effects of curcumin on multi drug resistance associated protein (MRP1) in retinoblastoma cells. *Bioinformation* **2012**, *8*, 13-19.
[45] Li, Q.-C.; Liang, Y.; Hu, G.-R.; Tian, Y. Enhanced therapeutic efficacy and amelioration of cisplatin-induced nephrotoxicity by quercetin in 1, 2-dimethyl hydrazine-induced colon cancer in rats. *Indian Journal of Pharmacology* **2016**, *48*, 168.
[46] Kovach, J.; Moertel, C.; Schutt, A.; Reitemeier, R.; Hahn, R. Phase II study of cis-diamminedichloroplatinum (NSC-119875) in advanced carcinoma of the large bowel. *Cancer Chemotherapy Reports. Part 1* **1972**, *57*, 357-359.
[47] Friedlander, M.; Kaye, S.; Sullivan, A.; Atkinson, K.; Elliott, P.; Coppleson, M.; Houghton, R.; Solomon, J.; Green, D.; Russell, P. Cervical carcinoma: a drug-responsive tumor—experience with combined cisplatin, vinblastine, and bleomycin therapy. *Gynecologic Oncology* **1983**, *16*, 275-281.
[48] Prestayko, A.; d'Aoust, J.; Issell, B.; Crooke, S. Cisplatin (cis-diamminedichloroplatinum II). *Cancer Treatment Reviews* **1979**, *6*, 17-39.
[49] Hashmi, H.; Maqbool, A.; Ahmed, S.; Ahmed, A.; Sheikh, K.; Ahmed, A. Concurrent cisplatin-based chemoradiation in squamous cell carcinoma of cervix. *Journal of the College of Physicians and Surgeons-Pakistan: JCPSP* **2016**, *26*, 302-305.
[50] Jendželovská, Z.; Jendželovský, R.; Hiľovská, L.; Kovaľ, J.; Mikeš, J.; Fedoročko, P. Single pre-treatment with hypericin, a St. John's wort secondary metabolite, attenuates cisplatin-and mitoxantrone-induced cell death in A2780, A2780cis and HL-60 cells. *Toxicology in Vitro* **2014**, *28*, 1259-1273.
[51] Xu, H.; Xu, L.; Hao, J.; Qin, C.; Liu, H. Expression of P-glycoprotein and multidrug resistance-associated protein is associated with multidrug resistance in gastric cancer. *Journal of International Medical Research* **2010**, *38*, 34-42.
[52] He, G.; He, G.; Zhou, R.; Pi, Z.; Zhu, T.; Jiang, L.; Xie, Y. Enhancement of cisplatin-induced colon cancer cells apoptosis by shikonin, a natural inducer of ROS *in vitro* and *in vivo*. *Biochemical and biophysical research communications***2016**, *469*, 1075-1082.
[53] Sui, X.; Luo, C.; Wang, C.; Zhang, F.; Zhang, J.; Guo, S. Graphene quantum dots enhance anticancer activity of cisplatin via increasing its cellular and nuclear uptake. *Nanomedicine: Nanotechnology, Biology and Medicine* **2016**.

[54] Desbois, N.; Pertuit, D.; Moretto, J.; Cachia, C.; Chauffert, B.; Bouyer, F. Cis-dichloroplatinum (II) complexes tethered to dibenzo [c, h][1, 6] naphthyridin-6-ones: synthesis and cytotoxicity in human cancer cell lines in vitro. *European Journal of Medicinal Chemistry* **2013**, *69*, 719-727.

[55] Lee, Y.; Kim, Y. J.; Choi, Y. J.; Lee, J. W.; Lee, S.; Chung, H. W. Enhancement of cisplatin cytotoxicity by benzyl isothiocyanate in HL-60 cells. *Food and Chemical Toxicology* **2012**, *50*, 2397-2406.

[56] Roy, M.; Mukherjee, S. Reversal of resistance towards cisplatin by curcumin in cervical cancer cells. *Asian Pacific Journal of Cancer Prevention: APJCP* **2013**, *15*, 1403-1410.

[57] Neumann, W.; Crews, B. C.; Sárosi, M. B.; Daniel, C. M.; Ghebreselasie, K.; Scholz, M. S.; Marnett, L. J.; Hey-Hawkins, E. Conjugation of cisplatin analogues and cyclooxygenase inhibitors to overcome cisplatin resistance. *ChemMedChem* **2015**, *10*, 183-192.

[58] Wang, Y.; Yang, J.; Yi, J. Redox sensing by proteins: oxidative modifications on cysteines and the consequent events. *Antioxidants & Redox Signaling* **2012**, *16*, 649-657.

[59] Pariente, R.; Pariente, J. A.; Rodríguez, A. B.; Espino, J. Melatonin sensitizes human cervical cancer HeLa cells to cisplatin-induced cytotoxicity and apoptosis: effects on oxidative stress and DNA fragmentation. *Journal of Pineal Research* **2016**, *60*, 55-64.

[60] Galluzzi, L.; Senovilla, L.; Vitale, I.; Michels, J.; Martins, I.; Kepp, O.; Castedo, M.; Kroemer, G. Molecular mechanisms of cisplatin resistance. *Oncogene* **2012**, *31*, 1869-1883.

[61] Liu, X.; Liu, S.; Jiang, J.; Zhang, X.; Zhang, T. Inhibition of the JNK signaling pathway increases sensitivity of hepatocellular carcinoma cells to cisplatin by down-regulating expression of P-glycoprotein. *European Review for Medical and Pharmacological Sciences* **2016**, *20*, 1098-1108.

[62] Ormerod, M.; O'neill, C.; Robertson, D.; Harrap, K. Cisplatin induces apoptosis in a human ovarian carcinoma cell line without concomitant internucleosomal degradation of DNA. *Experimental Cell Research* **1994**, *211*, 231-237.

[63] Ma, S.; Tan, W.; Du, B.; Liu, W.; Li, W.; Che, D.; Zhang, G. Oridonin effectively reverses cisplatin drug resistance in human ovarian cancer cells via induction of cell apoptosis and inhibition of matrix metalloproteinase expression. *Molecular Medicine Reports* **2016**, *13*, 3342-3348.

[64] Gołuński, G.; Woziwodzka, A.; Iermak, I.; Rychłowski, M.; Piosik, J. Modulation of acridine mutagen ICR191 intercalation to DNA by methylxanthines—analysis with mathematical models. *Bioorganic & Medicinal Chemistry* **2013**, *21*, 3280-3289.

[65] Woziwodzka, A.; Gwizdek-Wiśniewska, A.; Piosik, J. Caffeine, pentoxifylline and theophylline form stacking complexes with IQ-type heterocyclic aromatic amines. *Bioorganic Chemistry* **2011**, *39*, 10-17.

[66] Woziwodzka, A.; Gołuński, G.; Wyrzykowski, D.; Kaźmierkiewicz, R.; Piosik, J. Caffeine and other methylxanthines as interceptors of food-borne aromatic mutagens: inhibition of Trp-P-1 and Trp-P-2 mutagenic activity. *Chemical Research in Toxicology* **2013**, *26*, 1660-1673.

[67] Gołuński, G.; Borowik, A.; Derewońko, N.; Kawiak, A.; Rychłowski, M.; Woziwodzka, A.; Piosik, J. Pentoxifylline as a modulator of anticancer drug doxorubicin. Part II: Reduction of doxorubicin DNA binding and alleviation of its biological effects. *Biochimie* **2016**, *123*, 95-102.

[68] Gołuński, G.; Borowik, A.; Lipińska, A.; Romanik, M.; Derewońko, N.; Woziwodzka, A.; Piosik, J. Pentoxifylline affects idarubicin binding to DNA. *Bioorganic Chemistry* **2016**, *65*, 118-125.

[69] Orel, V.; Shevchenko, A.; Romanov, A.; Tselepi, M.; Mitrelias, T.; Barnes, C. H.; Burlaka, A.; Lukin, S.; Shchepotin, I. Magnetic properties and antitumor effect of nanocomplexes of iron oxide and doxorubicin. *Nanomedicine: Nanotechnology, Biology and Medicine* **2015**, *11*, 47-55.

[70] Prylutska, S.; Korolovych, V.; Prylutskyy, Y. I.; Evstigneev, M.; Ritter, U.; Scharff, P. Tumor-inhibitory effect of C_{60} fullerene complex with doxorubicin. *Nanomedicine and Nanobiology* **2015**, *2*, 49-53.

[71] Liu, X.; Liu, Y.; Hao, J.; Zhao, X.; Lang, Y.; Fan, F.; Cai, C.; Li, G.; Zhang, L.; Yu, G. *In vivo* anti-cancer mechanism of low-molecular-weight fucosylated chondroitin sulfate (LFCS) from Sea Cucumber Cucumaria frondosa. *Molecules* **2016**, *21*, 625.

[72] Xu, Y.-Z.; Li, Y.-H.; Lu, W.-J.; Lu, K.; Wang, C.-T.; Li, Y.; Lin, H.-J.; Kan, L.-X.; Yang, S.-Y.; Wang, S.-Y. YL4073 is a potent autophagy-stimulating antitumor agent in an in vivo model of Lewis lung carcinoma. *Oncology Reports* **2016**, *35*, 2081-2088.

[73] Peng, X. C.; Chen, X. X.; Zhang, Y.; Wang, H. J.; Feng, Y. A novel inhibitor of Rho GDP‐dissociation inhibitor α improves the therapeutic efficacy of paclitaxel in Lewis lung carcinoma. *Biomedical Reports* **2015**, *3*, 473-477.

[74] Fan, S.; Xu, Y.; Li, X.; Tie, L.; Pan, Y.; Li, X. Opposite angiogenic outcome of curcumin against ischemia and Lewis lung cancer models: *in silico, in vitro* and *in vivo* studies. *Biochimica et Biophysica Acta (BBA)-Molecular Basis of Disease* **2014**, *1842*, 1742-1754.

[75] Niu, P.-G.; Zhang, Y.-X.; Shi, D.-H.; Liu, Y.; Chen, Y.-Y.; Deng, J. Cardamonin inhibits metastasis of Lewis lung carcinoma cells by decreasing mTOR activity. *PloS One* **2015**, *10*, e0127778.

[76] Liu, Y.-Z.; Yang, C.-M.; Chen, J.-Y.; Liao, J.-W.; Hu, M.-L. Alpha-carotene inhibits metastasis in Lewis lung carcinoma *in vitro*, and suppresses lung metastasis and tumor growth in combination with taxol in tumor xenografted C57BL/6 mice. *The Journal of Nutritional Biochemistry* **2015**, *26*, 607-615.

[77] Das, S. K.; Eder, S.; Schauer, S.; Diwoky, C.; Temmel, H.; Guertl, B.; Gorkiewicz, G.; Tamilarasan, K. P.; Kumari, P.; Trauner, M. Adipose triglyceride lipase contributes to cancer-associated cachexia. *Science* **2011**, *333*, 233-238.

[78] Tsoli, M.; Robertson, G. Cancer cachexia: malignant inflammation, tumorkines, and metabolic mayhem. *Trends in Endocrinology & Metabolism* **2013**, *24*, 174-183.

[79] Porporato, P. Understanding cachexia as a cancer metabolism syndrome. *Oncogenesis***2016**, *5*, e200.

[80] Perego, P.; Righetti, S.; Supino, R.; Delia, D.; Caserini, C.; Carenini, N.; Bedogne, B.; Broome, E.; Krajewski, S.; Reed, J. Role of apoptosis and apoptosis-related proteins in the cisplatin-resistant phenotype of human tumor cell lines. *Apoptosis* **1997**, *2*, 540-548.

[81] Jinushi, M. Immune regulation of therapy-resistant niches: emerging targets for improving anticancer drug responses. *Cancer and Metastasis Reviews* **2014**, *33*, 737-745.

[82] D'Arena, G.; Deaglio, S.; Laurenti, L.; De Martino, L.; De Feo, V.; M Fusco, B.; M Carella, A.; Cascavilla, N.; Musto, P. Targeting regulatory t cells for anticancer therapy. *Mini Reviews in Medicinal Chemistry* **2011**, *11*, 480-485.

[83] R Shurin, M.; Naiditch, H.; W Gutkin, D.; Umansky, V.; Shurin, G. ChemoImmunoModulation: immune regulation by the antineoplastic chemotherapeutic agents. *Current Medicinal Chemistry* **2012**, *19*, 1792-1803.

[84] Skivka, L. M.; Fedorchuk, O. G.; Bezdeneznykh, N. O.; Lykhova, O. O.; Semesiuk, N. I.; Kudryavets, Y. I.; Malanchuk, O. M. The effect of antineoplastic drug NSC631570 on immunogenicity of B16 melanoma. *Journal of Experimental and Integrative Medicine* **2014**, *4*, 93-105.

[85] Fedorchuk, O. G.; Pyaskovskaya, O. M.; Skivka, L. M.; Gorbik, G. V.; Trompak, O. O.; Solyanik, G. I. Paraneoplastic syndrome in mice bearing high-angiogenic variant of Lewis lung carcinoma: relations with tumor derived VEGF. *Cytokine* **2012**, *57*, 81-88.

[86] Yang, X.; Ebrahimi, A.; Li, J.; Cui, Q. Fullerene–biomolecule conjugates and their biomedicinal applications. *International Journal of Nanomedicine* **2014**, *9*, 77.

[87] Turabekova, M.; Rasulev, B.; Theodore, M.; Jackman, J.; Leszczynska, D.; Leszczynski, J. Immunotoxicity of nanoparticles: a computational study suggests that CNTs and C 60 fullerenes might be recognized as pathogens by Toll-like receptors. *Nanoscale* **2014**, *6*, 3488-3495.

[88] Prylutska, S.; Grynyuk, I.; Grebinyk, S.; Matyshevska, O.; Prylutskyy, Y. I.; Ritter, U.; Siegmund, C.; Scharff, P. Comparative study of biological action of fullerenes C_{60} and carbon nanotubes in thymus cells. *Materialwissenschaft Und Werkstofftechnik* **2009**, *40*, 238-241.

[89] Prylutskyy, Yu.; Petrenko, V.; Ivankov, O.; Kyzyma, O.; Bulavin, L.; Litsis, O.; Evstigneev, M.; Cherepanov, V.; Naumovets, A.; Ritter, U. On the origin of C_{60} fullerene solubility in aqueous solution. *Langmuir* **2014**, *30*, 3967-3970.

[90] Ritter, U.; Prylutskyy, Y.; Evstigneev, M.; Davidenko, N.; Cherepanov, V.; Senenko, A.; Marchenko, O.; Naumovets, A. Structural features of highly stable reproducible C_{60} fullerene aqueous colloid solution probed by various techniques. *Fullerenes, Nanotubes and Carbon Nanostructures* **2015**, *23*, 530-534.

[91] Blanton, T.; Barnes, C.; Lelental, M. Preparation of silver behenate coatings to provide low-to mid-angle diffraction calibration. *Journal of Applied Crystallography* **2000**, *33*, 172-173.

[92] Franke, D.; Kikhney, A. G.; Svergun, D. I. Automated acquisition and analysis of small angle X-ray scattering data. *Nuclear Instruments and Methods in Physics Research Section A: Accelerators, Spectrometers, Detectors and Associated Equipment* **2012**, *689*, 52-59.

[93] Svergun, D. Determination of the regularization parameter in indirect-transform methods using perceptual criteria. *Journal of Applied Crystallography* **1992**, *25*, 495-503.

[94] Li, J.; Jaimes, K. F.; Aller, S. G. Refined structures of mouse P-glycoprotein. *Protein Science* **2014**, *23*, 34-46.

[95] Ramaen, O.; Leulliot, N.; Sizun, C.; Ulryck, N.; Pamlard, O.; Lallemand, J.-Y.; van Tilbeurgh, H.; Jacquet, E. Structure of the human multidrug resistance protein 1 nucleotide binding domain 1 bound to Mg 2+/ATP reveals a non-productive catalytic site. *Journal of Molecular Biology* **2006**, *359*, 940-949.

[96] Vedadi, M.; Lew, J.; Artz, J.; Amani, M.; Zhao, Y.; Dong, A.; Wasney, G. A.; Gao, M.; Hills, T.; Brokx, S. Genome-scale protein expression and structural biology of Plasmodium falciparum and related Apicomplexan organisms. *Molecular and Biochemical Parasitology* **2007**, *151*, 100-110.

[97] Warren, G. L.; Andrews, C. W.; Capelli, A.-M.; Clarke, B.; LaLonde, J.; Lambert, M. H.; Lindvall, M.; Nevins, N.; Semus, S. F.; Senger, S. A critical assessment of docking programs and scoring functions. *Journal of Medicinal Chemistry* **2006**, *49*, 5912-5931.

[98] Shen, D.-W.; Cardarelli, C.; Hwang, J.; Cornwell, M.; Richert, N.; Ishii, S.; Pastan, I.; Gottesman, M. Multiple drug-resistant human KB carcinoma cells independently selected for high-level resistance to colchicine, adriamycin, or vinblastine show changes in expression of specific proteins. *Journal of Biological Chemistry* **1986**, *261*, 7762-7770.

[99] McGrath, T.; Center, M. S. Mechanisms of multidrug resistance in HL60 cells: evidence that a surface membrane protein distinct from P-glycoprotein contributes to reduced cellular accumulation of drug. *Cancer Research* **1988**, *48*, 3959-3963.

[100] Walker, P. R.; Kwast-Welfeld, J.; Gourdeau, H.; Leblanc, J.; Neugebauer, W.; Sikorska, M. Relationship between apoptosis and the cell cycle in lymphocytes: roles of protein kinase C, tyrosine phosphorylation, and AP1. *Experimental Cell Research* **1993**, *207*, 142-151.

[101] Mortelmans, K.; Zeiger, E. The Ames Salmonella/microsome mutagenicity assay. *Mutation Research/Fundamental and Molecular Mechanisms of Mutagenesis* **2000**, *455*, 29-60.

Figure 1. Small-angle X-ray scattering analysis of obtained C_{60} fullerene and Cis complex (C_{60}+Cis complex). Experimental Small-angle X-ray scattering curves (points) for the C_{60} fullerene (red) and the C_{60}+Cis complex (green) aqueous systems. Solid lines correspond to the model curves obtained by the indirect Fourier transformation procedure. In the inset normalized pair distance distribution functions as a result of the indirect Fourier transformation procedure for scattering from the C_{60} fullerene (red) and the C_{60}+Cis complex (green) aqueous systems are shown.

Figure 2. Molecular docking of C_{60} fullerene to P-glycoprotein (P-gp), Multidrug resistance protein 1 (MRP-1) and Multidrug resistance protein 2 (MRP-2). **Panel A:** Hypothetic geometric image of the C_{60} fullerene binding to P-gp in four potentially possible positions 1, 2, 3 and 4; **Panel B**: Potential binding sites for C_{60} fullerene binding to MRP-1; **Panel C**: Potential binding sites for C_{60}fullerene binding to MRP-2.

Figure 3. Cytotoxic activity of C_{60} fullerene and Cis complex (C_{60}+Cis complex) towards human colon and cervix cancer cell lines. The graphs present the effects of the treatment with C_{60} fullerene (presented in gray), Cis (presented in black) and the C_{60}+Cis complex (presented in crossed gray). Cell viability was estimated using the trypan blue exclusion assay. The effect of Cis and C_{60}+Cis complex on cell growth was plotted relative to the untreated control. Data are given relative to the untreated control samples and represent the mean +/- SD of three independent experiments. *$p<0.05$ relative to control, **$p<0.01$ relative to control, ***$p<0.0001$ relative to control, unpaired t-test. Significance levels indicated directly above bars refer to the comparison with the respective vehicle-treated controls.

Figure 4. Cytotoxic activity of C_{60} fullerene and Cis complex (C_{60}+Cis complex) towards leukaemia cell lines. The graphs present the effects of the treatment with C_{60} fullerene (presented in gray), Cis (presented in black) and C_{60}+Cis complex (presented in crossed gray). Cell viability was estimated using trypan blue exclusion assay. The effect of Cis and C_{60}+Cis complex on cell growth was plotted relative to the untreated control. Data are given relative to the untreated control samples and represent the mean +/- SD of three independent experiments. *$p<0.05$ relative to control, **$p<0.01$ relative to control, ***$p<0.0001$ relative to control, unpaired t-test. Significance levels indicated directly above bars refer to the comparison with the respective vehicle-treated controls.

Figure 5. Chromatin hypercondensation studies in the human cervix carcinoma cell line KB-3-1 treated with C_{60} fullerene and Cis complex (C_{60}+Cis complex). DAPI staining, 24 h incubation with the drugs. **Panel A**: control; **Panel B**: Cis, 15 μM; **Panel C**: Cis, 20 μM; **Panel D**: C_{60} fullerene, 20 μM; **Panel E**: C_{60}+Cis complex, 15 μM; **Panel F**: C_{60}+Cis complex, 20 μM.

Figure 6. Flow cytometry analysis of apoptosis induction (**Panel A**) and cell cycle distribution (**Panel B**) in human HL-60/adr (MRP-1+) cells induced by C_{60} fullerene and Cis complex (C_{60}+Cis complex). Apoptosis analysis and cell cycle studies were conducted using AnnexinV-FITC/PI assay and PI staining, respectively. Data are given relative to the untreated control samples and represent the mean +/- SD of three independent experiments. *$p<0.05$ relative to control, **$p<0.01$ relative to control, unpaired t-test. Significance levels indicated directly above bars refer to the comparison with the respective vehicle-treated controls.

Figure 7. Ames mutagenicity test of Cis and C_{60} fullerene and Cis complex (C_{60}+Cis complex) in *Salmonella typhimurium* TA102 strain. Overnight cultures of *S. typhimurium* TA102 were treated with 500 ng Cis or a mixture of 500 ng Cis with 0.01-10 μg C_{60} fullerene,

and incubated for 4 h. Subsequently, bacteria were spread on glucose minimal plates and the revertants were counted after 48 h cultivation. Results are presented as means from three plates ± SD; *- values significantly different from cells treated with Cis alone ($p<0.05$).

Figure 8. Changes in tumor volume in Lewis lung carcinoma bearing mice treated with the C_{60} fullerene, Cis or C_{60} fullerene and Cis complex (C_{60}+Cis complex).

Suppl. Figure 1. Comparison of cytotoxic activity of C_{60}+Cis complexes with different drug-to-carrier ratios (N1 (1:0.6), N2 (1:1.2), N3 (1:2.4), and N4 (1:4.8)) towards human leukemia cells of HL-60/wt line and its drug-resistant subline HL-60/vinc (P-gp+). The effect of analyzed substances on cell growth was plotted as a percentage of control (untreated cells). Graphs represent the mean values +/- standard deviation of three independent experiments done in triplicates. **,*** - values significantly different from cells treated with Cis alone ($p<0.01$, $p<0.001$, respectively).

Table 1. Energy characteristics for the C_{60} fullerene+P-glycoprotein simulated complex, dependent on the binding position

Positions	***FreE***, kJ/mol	***Cntc***, kJ/mol	***Bump***, kJ/mol
Extra-Cell (1)	-23.5	-70	19.1
Native binding site (2)	-49.1	-78.5	1.6
Membrane Interior (3)	-29.5	-72.1	8.3
Intra-Cell (4)	-22.2	-54	6.2

FreE: the energy of complex; ***Cntc***: the energy of interaction between the C_{60} fullerene and protein; ***Bump***: the energy of steric clashes between the C_{60} fullerene and protein

Table 2. Tumor growth inhibition index (TGII, %*) calculated for treated Lewis lung carcinoma bearing mice

Animal group	Day after tumor cell transplantation			
	11	14	17	20
Group 1 (C_{60} fullerene injection), n=10	21±2	33±2	35±3	17±1
Group 2 (Cisplatin injection), n=10	51±4	49±3	48±3	18±2
Group 3 (C_{60} fullerene+Cisplatin injection), n=10	53±3	59±3	52±1	36±2

*$p<0.05$ vs control

Table 3. Effects of C_{60}+Cis complex on the metastasizing of the Lewis lung carcinoma in mice

Animal group	The number of tumor foci per mice	Total volume of lung metastases (mm^3) per mice	An average volume of a single metastatic focus (mm^3)
Control group, n=10	13	112±8	8.6±0.6
Group 1 (C_{60} fullerene injection), n=10	7	30±2*	4.3±0.3*
Group 2 (Cisplatin injection), n=10	12	48±3*	4.0±0.3*
Group 3 (C_{60} fullerene+Cisplatin injection), n=10	9	28±2*	3.1±0.2*

*p<0.05 - vs *intact* animals

Table 4. Effects of C_{60}+Cis complex on cachexia of the Lewis lung carcinoma bearing mice

Animal group	Weight (g)
Intact animals, n=10	18.1±0.9
Control group, n=10	13.0±1.1*
Group 1 (C_{60} fullerene injection), n=10	14.2±1.0*
Group 2 (Cisplatin injection), n=10	11.7±0.9*
Group 3 (C_{60} fullerene+Cisplatin injection), n=10	15.3±1.2*

*p<0.05 - vs *intact* animals

Table 5. Effects of C_{60}+Cis complex on spleen and thymus of the Lewis lung carcinoma-bearing mice

Animal group	Total spleen weight (g)	Splenic index	Total thymus weight (g)	Thymic index
Intact animals, n=10	0.091±0.007*	5	0.038±0.003	2.1
Control group, n=10	0.155±0.010	9.1	0.039±0.004	2.3
Group 1 (C_{60} fullerene injection), n=10	0.111±0.009*	6.5	0.011±0.001*	0.6
Group 2 (Cisplatin injection), n=10	0.112±0.009*	7.2	0.028±0.002*	1.8
Group 3 (C_{60} fullerene+ Cisplatin injection), n=10	0.117±0.008*	6.4	0.020±0.001*	1.1

*p<0.05 - vs *control* tumor bearing mice

Fig. 1

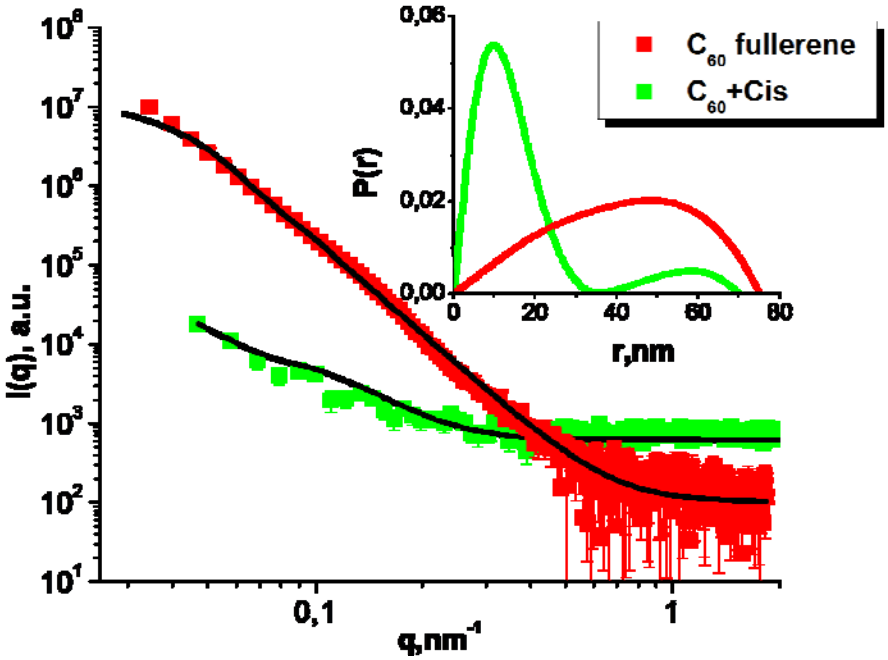

Fig. 2A

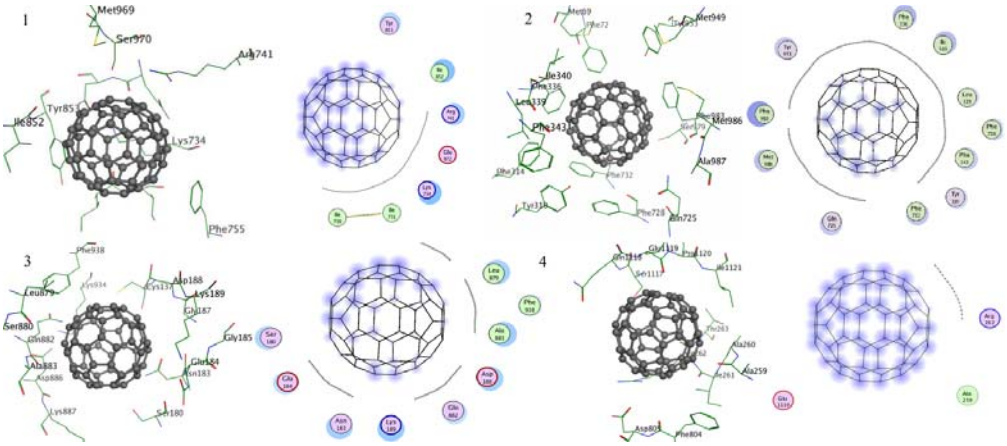

Fig. 2B

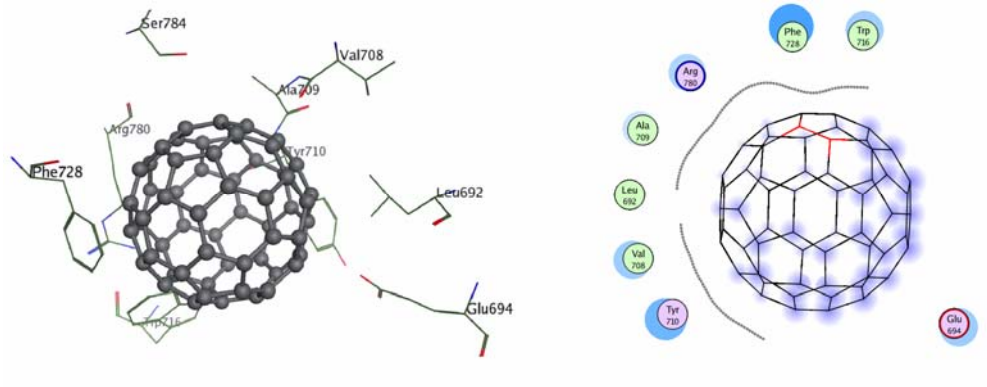

Fig. 2C

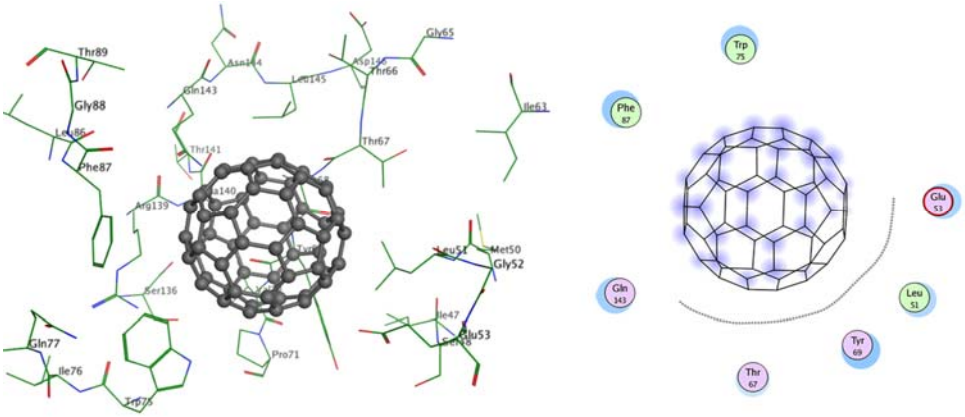

Fig. 3

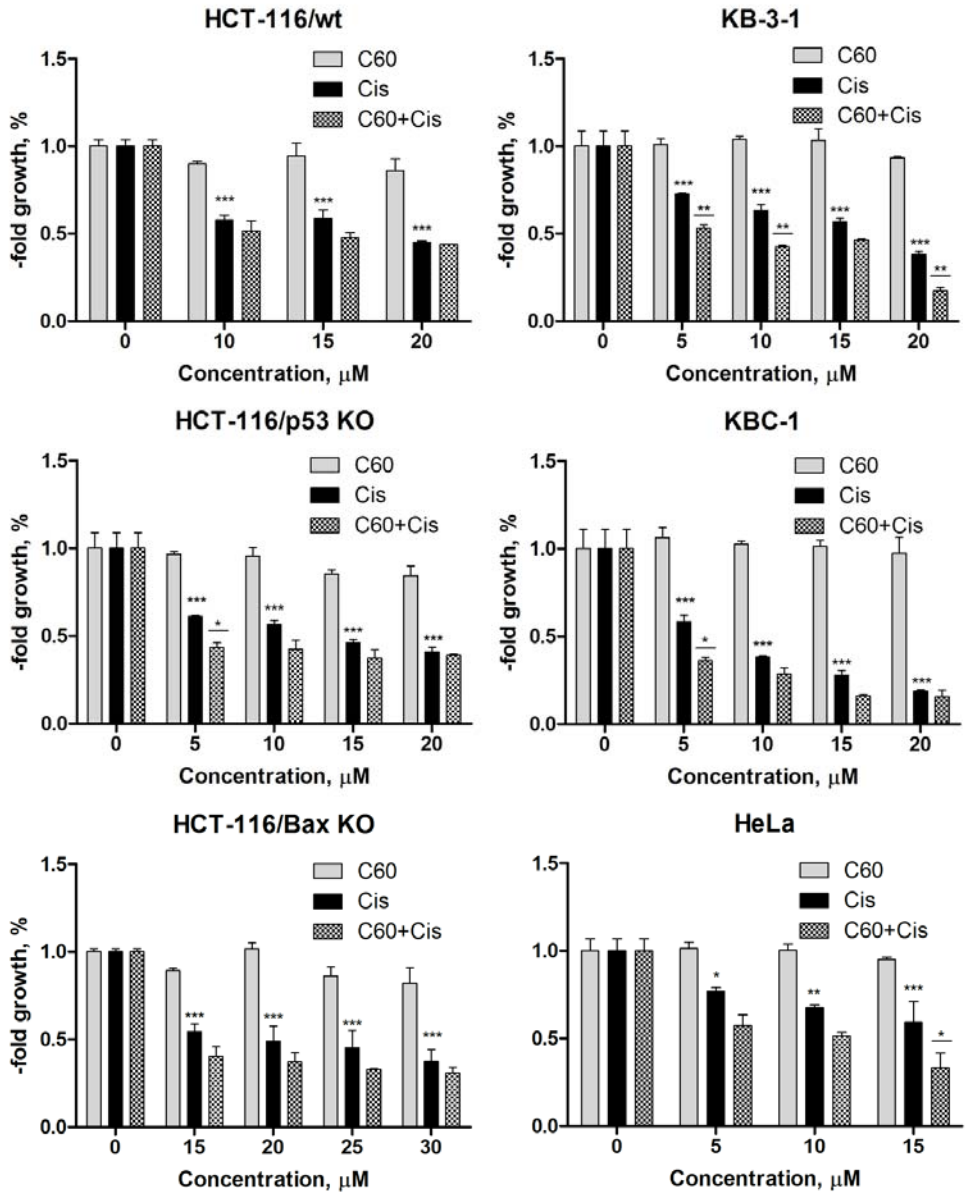
HCT-116/wt
KB-3-1
HCT-116/p53 KO
KBC-1
HCT-116/Bax KO
HeLa
C60
Cis
C60+Cis
-fold growth, %
Concentration, μM

Fig. 4

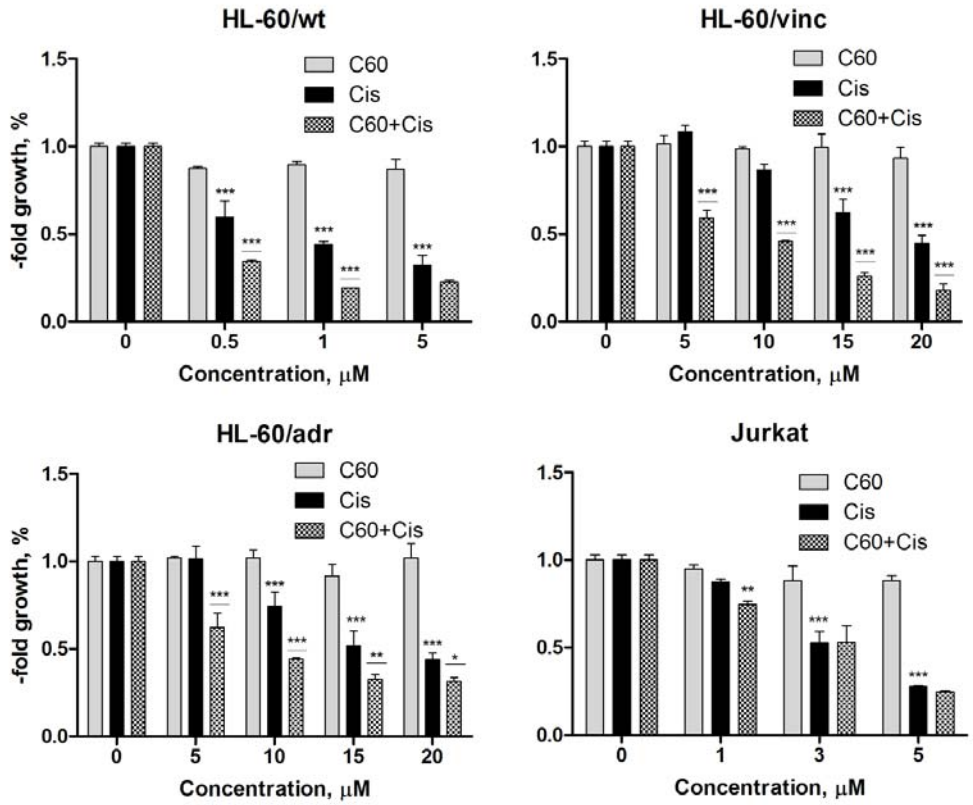
HL-60/wt
HL-60/vinc
HL-60/adr
Jurkat
C60
Cis
C60+Cis
-fold growth, %
Concentration, μM
1.5
1.0
0.5
0.0
0
0.5
1
5
10
15
20
3
***
**
*

Fig. 5

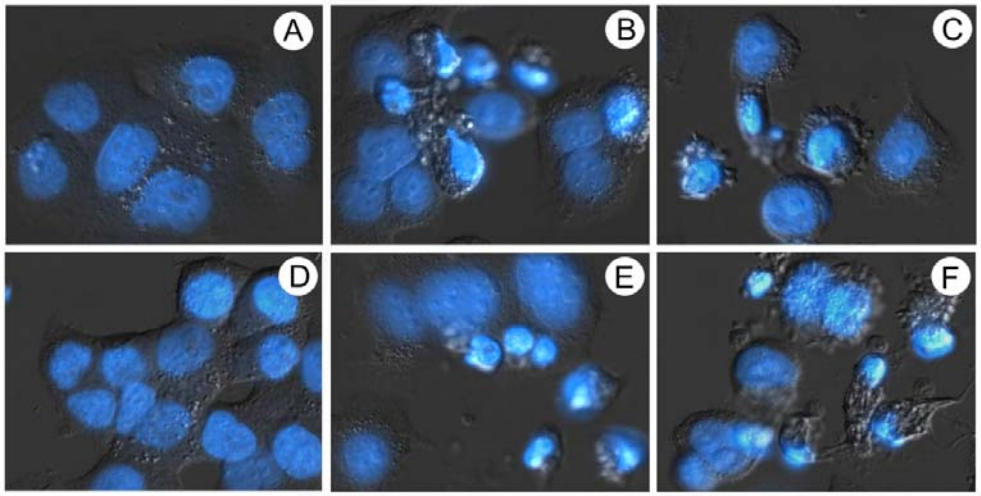

Fig. 6

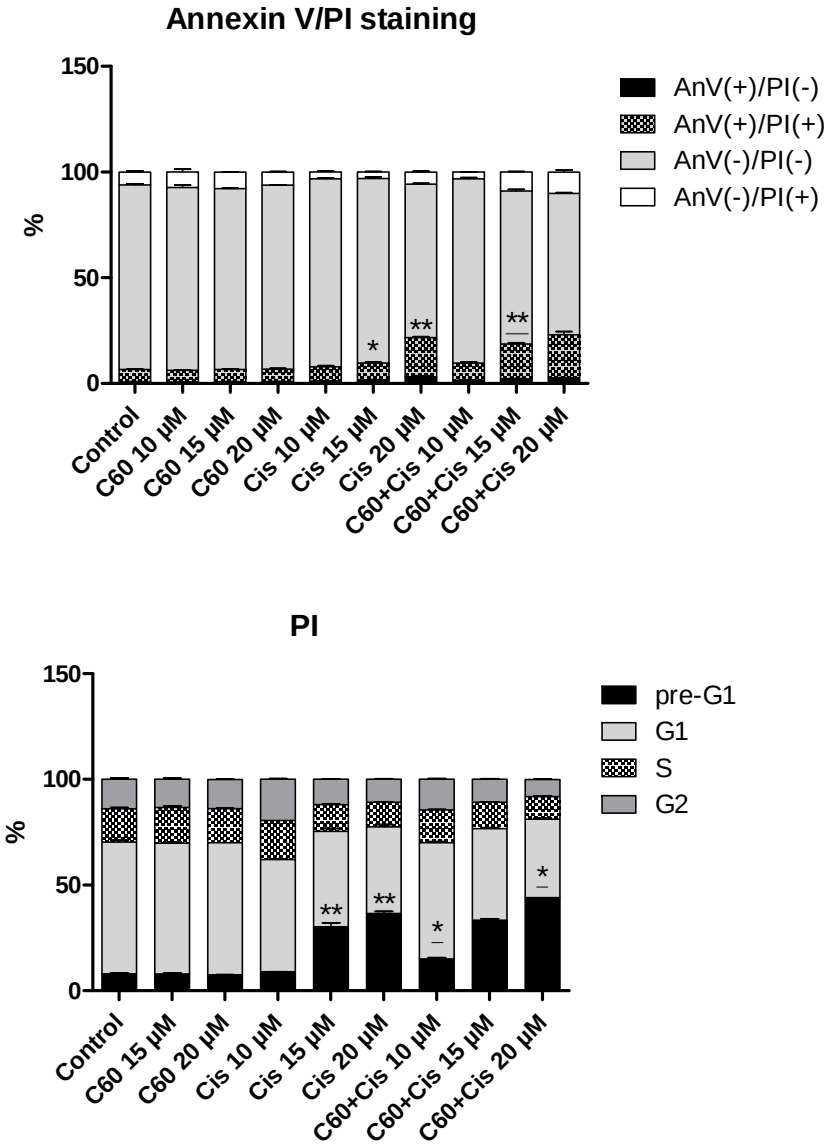
Annexin V/PI staining
150
100
50
0
%
AnV(+)/PI(-)
AnV(+)/PI(+)
AnV(-)/PI(-)
AnV(-)/PI(+)
*
**
**
Control
C60 10 μM
C60 15 μM
C60 20 μM
Cis 10 μM
Cis 15 μM
Cis 20 μM
C60+Cis 10 μM
C60+Cis 15 μM
C60+Cis 20 μM
PI
150
100
50
0
%
pre-G1
G1
S
G2
**
**
*
*
Control
C60 15 μM
C60 20 μM
Cis 10 μM
Cis 15 μM
Cis 20 μM
C60+Cis 10 μM
C60+Cis 15 μM
C60+Cis 20 μM

Fig. 7

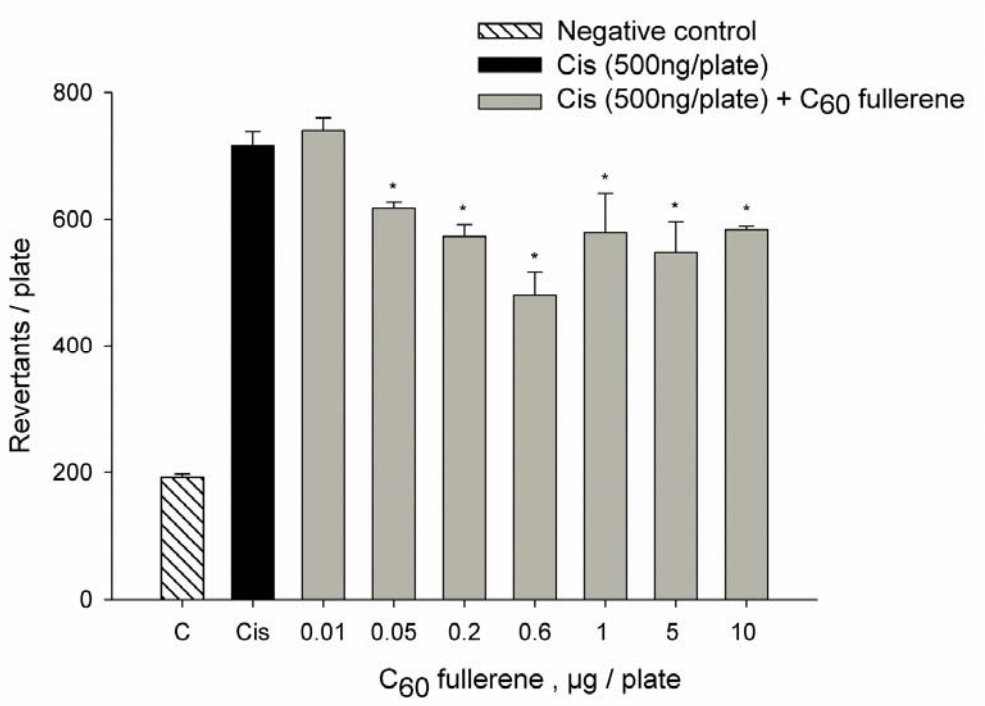
Negative control
Cis (500ng/plate)
Cis (500ng/plate) + C60 fullerene
Revertants / plate
800
600
400
200
0
C
Cis
0.01
0.05
0.2
0.6
1
5
10
C60 fullerene , µg / plate

Fig. 8

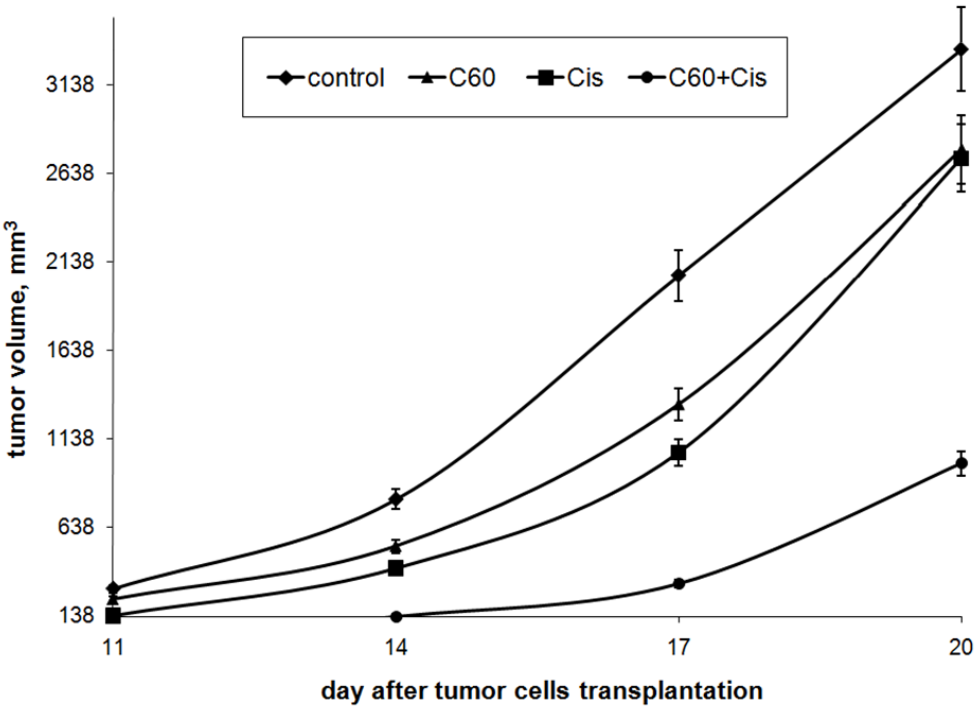
control
C60
Cis
C60+Cis
3138
2638
2138
1638
1138
638
138
tumor volume, mm3
11
14
17
20
day after tumor cells transplantation

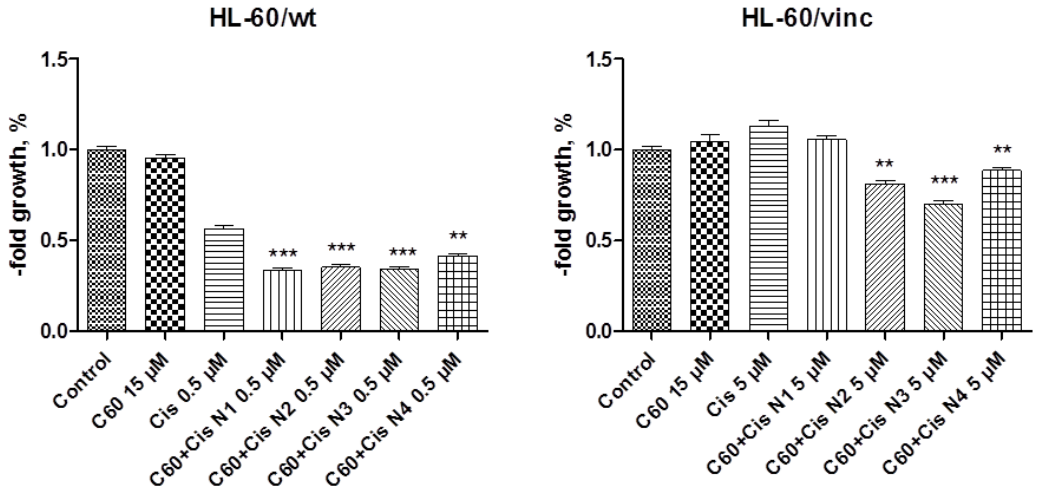
HL-60/wt
-fold growth, %
1.5
1.0
0.5
0.0
***
***
***
**
Control
C60 15 μM
Cis 0.5 μM
C60+Cis N1 0.5 μM
C60+Cis N2 0.5 μM
C60+Cis N3 0.5 μM
C60+Cis N4 0.5 μM
HL-60/vinc
-fold growth, %
1.5
1.0
0.5
0.0
**
***
**
Control
C60 15 μM
Cis 5 μM
C60+Cis N1 5 μM
C60+Cis N2 5 μM
C60+Cis N3 5 μM
C60+Cis N4 5 μM

Suppl. Fig. 1.